

University of Montana

ScholarWorks at University of Montana

Graduate Student Theses, Dissertations, &
Professional Papers

Graduate School

2015

DYNAMIC MOTIONS OF THE ALPHA SUBUNIT OF HETEROTRIMERIC G PROTEINS IN THE NUCLEOTIDE- AND RIC-8A-BOUND STATES

Labe Adam Black
The University of Montana

Follow this and additional works at: <https://scholarworks.umt.edu/etd>

Let us know how access to this document benefits you.

Recommended Citation

Black, Labe Adam, "DYNAMIC MOTIONS OF THE ALPHA SUBUNIT OF HETEROTRIMERIC G PROTEINS IN THE NUCLEOTIDE- AND RIC-8A-BOUND STATES" (2015). *Graduate Student Theses, Dissertations, & Professional Papers*. 4610.
<https://scholarworks.umt.edu/etd/4610>

This Dissertation is brought to you for free and open access by the Graduate School at ScholarWorks at University of Montana. It has been accepted for inclusion in Graduate Student Theses, Dissertations, & Professional Papers by an authorized administrator of ScholarWorks at University of Montana. For more information, please contact scholarworks@mso.umt.edu.

DYNAMIC MOTIONS OF THE ALPHA SUBUNIT OF HETEROTRIMERIC G PROTEINS

IN THE NUCLEOTIDE- AND RIC-8A-BOUND STATES

By

Labe Adam Black

Master of Science, Bucknell University, Lewisburg, PA, 08648

Bachelor of Science, Rider University, Lawrenceville, NJ, 17837

Dissertation

presented in partial fulfillment of the requirements
for the degree of

Doctor of Philosophy
in Chemistry and Biochemistry

The University of Montana
Missoula, MT

Official Graduation Date July 2015

Approved by:

J.B. Alexander Ross
Dean of the Graduate School

J.B. Alexander Ross and Stephen R. Sprang, Co-Chairs
Department Chemistry and Biochemistry, Division of Biological Sciences

Edward Rosenberg
Department of Chemistry and Biochemistry

Christopher Palmer
Department Chemistry and Biochemistry

Bruce Bowler
Department Chemistry and Biochemistry

© COPYRIGHT

by

Labe A. Black

2015

All Rights Reserved

Table of Contents	Page Number
Abstract	1
Chapter 1: Introduction	3
<i>G proteins – function</i>	4
<i>G proteins – classification</i>	6
<i>Guanine Nucleotide-Exchange Factors (GEFs)</i>	6
<i>Structure of G Proteins</i>	8
<i>G Protein Dynamics</i>	10
<i>Ric-8</i>	11
<i>Dissertation Aims</i>	12
Hypothesis Statement	13
Chapter 2: Secondary Structural Dynamics of G α	14
Introduction	15
Methods	16
<i>Protein Expression and Purification</i>	16
<i>Protein Fluorescence Labeling</i>	18
<i>Gai1 Functional Assays</i>	18
<i>Experimental Setup and Data Collection</i>	19
<i>Fluorescent lifetime and time-resolved anisotropy measurements</i>	20
<i>Fluorescence Correlation Spectroscopy (FCS)</i>	22
<i>Error Analysis</i>	23
Results	23
<i>Gai1 Activity Assays of labeled protein</i>	23
<i>Fluorescence Anisotropy and FCS</i>	23
<i>“Wobble-in-a-cone” Model</i>	26
Discussion	29
<i>Individual Gai1 Mutant Depolarization Trends by Binding State</i>	29
<i>Comparison of Gai1 Mutant Depolarization Trends by Binding State</i>	34
<i>GDP-Bound State</i>	34
<i>Ric-8A-Bound State</i>	35
<i>GTP-Bound State</i>	38
Conclusion	39
Chapter 3: Conformational Changes of G α	41
Introduction	42
Methods	43
<i>Protein Expression and Purification</i>	43
<i>Protein Fluorescence Labeling</i>	44
<i>Experimental Setup and Data Collection</i>	44
<i>Ric-8A Binding and Nucleotide Exchange Assays</i>	45
<i>Steady-State GTP Hydrolysis Assay</i>	46
<i>Fluorescence Assay of GTP Binding</i>	46
<i>Fluorescence Correlation Spectroscopy (FCS)</i>	46
<i>Single-molecule Förster resonance energy transfer (smFRET)</i>	48
<i>3-Gaussian Model – Rates and Conformational Equilibria</i>	48

<i>Application of the Gopich-Szabo 3-Gaussian Model</i>	50
<i>Construction of FRET efficiency histograms using PIE</i>	52
<i>Brightness-Corrected FRET-Efficiency Histograms</i>	52
<i>Determination of Rates and Conformational Equilibria</i>	53
Results	53
<i>Biochemical activity of Alexa-Gai1 adducts</i>	53
<i>Global structural changes deduced from smFRET of freely diffusing proteins</i>	53
<i>Dynamics of Gα1 Structural Changes</i>	55
<i>Intra-Domain Dynamics</i>	56
<i>Inter-Domain Dynamics</i>	58
Discussion	61
<i>Intra-domain Conformational Dynamics</i>	62
<i>Inter-Domain Conformational Dynamics</i>	64
Conclusion	65
Chapter 4: Conclusion	68
Reference list	72
Figure List	
Figure 1 G Protein Guanine Nucleotide Exchange Cycle for the GEF Ric-8A and GPCRs	5
Figure 2 Schematic of the tertiary structure of G α 1	9
Figure 3 Segmental correlation times	28
Figure 4 Cone angles	28
Figure 5 Heat-map constructed from segmental correlation times	36
Figure 6 Heat-map constructed from segmental fraction β	37
Figure 7 Theoretical burst intensity trace of both donor and acceptor emission	51
Figure 8 Donor and acceptor channel brightness-corrected (γ -factor) FRET efficiency histograms	55
Figure 9 Time-dependent FRET efficiency histograms for intra- and inter-domain G α 1 mutants	60
Table List	
Table 1 Translational diffusion coefficients of G α 1	25
Table 2 Recovered parameters of globally fixed (ϕ_{global}) anisotropy decay curves for G α 1	27
Table 3 Rate and equilibrium parameters recovered from the 3-Gaussian model	58
Appendix	79

Title: DYNAMIC MOTIONS OF THE ALPHA SUBUNIT OF HETEROTRIMERIC G PROTEINS

IN THE NUCLEOTIDE- AND RIC-8A-BOUND STATES

Co-Chairpersons: J.B. Alexander Ross and Stephen R. Sprang

Abstract: The conformational changes and segmental dynamics involved in the α -subunit of heterotrimeric G proteins have been investigated for three separate binding states by using binning-time-dependent single-molecule Förster resonance energy transfer (smFRET) of freely diffusing proteins and time-resolved fluorescence anisotropy. The bound states include Ric-8A (Resistance to Inhibitors of Cholinesterase-8A (Miller, Emerson et al. 2000; Miller and Rand 2000; Tall, Krumins et al. 2003)), a guanine nucleotide exchange factor (GEF), and nucleotides GDP and GTP. To analyze the smFRET data, energy transfer efficiency histograms were constructed at binning times varied from 1,000 to 2,500 μ s. Then the conformational equilibria and rates of conformational change between end states (GTP-bound, GDP-bound, and Ric-8A-bound) were extracted using the 3-Gaussian model, developed by Gopich and Szabo (Gopich and Szabo 2007; Gopich and Szabo 2010). Using this model, we determined that intra- and inter-domain dynamics occur on the ms time scale. The Helical-Helical conformational changes are relatively small ($< 5 \text{ \AA}$), without observable influence from the binding partner (nucleotide or GEF). The intra Ras-like domain conformational changes are somewhat larger ($>5 \text{ \AA}$), and have distinct, multiple states regardless of binding partner (GTP, GDP and Ric-8A). The inter-domain conformational changes are much larger ($>40 \text{ \AA}$), and likewise exhibit distinct, multiple states that are binding-partner dependent.

Time-resolved fluorescence anisotropy resolved segmental motions of the binding states that occur on the ps-to-ns timescale. These analyses show secondary structural motions on the ns timescale are significantly different for the three states (GDP-, GTP- and GEF-bound), and map possible binding

sites and secondary structural conformational changes associated with GEF activity. These include a binding interface between $G\alpha$ and Ric-8A likely involving switch regions I and II, and possibly the hinge regions, specifically the amino-terminal of helix αA connecting the Ras-like and Helical domain. This region has significant conformational restraints when bound to Ric-8A, and the $\alpha 5$ helix leading to the C-terminus most likely is displaced through rotation and translation into the nucleotide-binding pocket, causing an increased rate of nucleotide exchange, similar to the light-activated rhodopsin G-protein-coupled receptor (Van Eps et al. 2006). Together, these data point to a preorganization mechanism, which explains the ability of GEFs to induce conformational changes that alter structural dynamics, thereby effectively enhancing nucleotide exchange activity in $G\alpha$.

Chapter 1

Introduction

G proteins – function: The ability for organisms to communicate with the external environment is critical for survival and reproduction. In multicellular organisms, communication between and within cells is predominantly governed by G protein signaling. G proteins receive and relay signals coming from 7-transmembrane surface receptors, G protein couple receptors (GPCRs), that span the cell membrane wall (Sprang 1995; Coleman and Sprang 1996; Sprang 1997; Sprang 1997; Gether and Kobilka 1998; Rohrer and Kobilka 1998; Seifert, Wenzel-Seifert et al. 1999; Hamm 2001; Sprang 2001; Cabrera-Vera, Vanhauwe et al. 2003; Preininger and Hamm 2004; Holinstat, Oldham et al. 2006; Oldham, Van Eps et al. 2006; Deupi and Kobilka 2007; Kobilka 2007; Oldham and Hamm 2007; Sprang 2007; Oldham and Hamm 2008; Granier and Kobilka 2012; Sprang and Elk 2012; Manglik and Kobilka 2014). These receptors receive external signals through interactions with external stimuli, such as binding ligands know as agonists, antagonists or inhibitors. Once a receptor receives the external signal it becomes activated. The activated receptor then relays the signal through the cell wall by coupling to guanine nucleotide-binding proteins, G proteins. Mechanistically, G proteins act as heterotrimeric holoenzymes that hydrolyze guanosine triphosphate (GTP) to guanosine diphosphate (GDP) in the $G\alpha$ subunit. $G\alpha$ acts as a signaling “switch” because signaling is quenched, or turned off when the enzyme hydrolyzes GTP to GDP. The receptor, however, can turn the signaling pathway back on by inducing the exchange of GDP for GTP, the rate-limiting step of the catalytic cycle. The receptor acts as a guanine-nucleotide exchange factor (GEF) that increases the rate at which GDP is exchanged for GTP in the alpha subunit of the heterotrimer. Figure 1 is a cartoon that depicts the G protein signaling cycle.

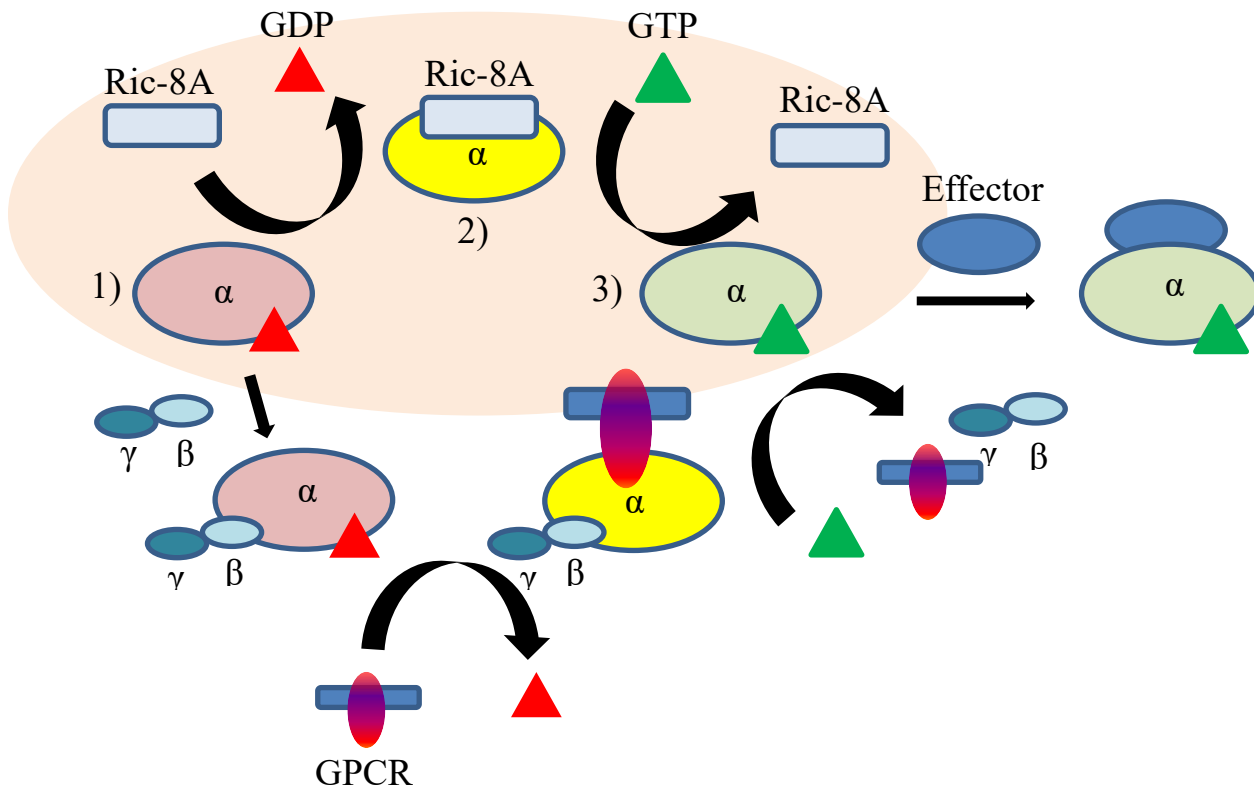


Figure 1 G Protein guanine nucleotide exchange cycle for the GEF Ric-8A and GPCRs 1) Gα bound to GDP, the inactive state. 2) Gα-GDP binds Ric-8A catalyzing the release of GDP. 3) Gα binds GTP and causes the dissociation from Ric-8A. Gα catalyzes the γ-phosphate cleavage of GTP, returning to the GDP-bound state completing the cycle. GPCRs act similarly but act only on G-protein heterotrimers (Kobilka 2007).

G proteins – classification: The alpha subunit of G protein heterotrimers ($G\alpha$) are separated into four classes based on their sequence similarity, function and effector they interact with. (1) $G\alpha_s$ interacts with adenylyl cyclase and stimulates cyclic-adenosine monophosphate (cAMP) production. (2) $G\alpha_i$ also interacts with adenylyl cyclase but inhibits cAMP production. (3) $G\alpha_q/11$ interacts with phospholipase C- β (PLC β) and (4) $G\alpha_{12/13}$ interacts with a subset of RhoGEFs that activate Rho, a small GTPase (Sprang 1997; Sprang 1997; Sprang 2009). Structurally, $G\alpha$ is composed of two domains: the Helical and Ras-like domain. There are common motifs in $G\alpha$ including the P-loop responsible for binding the nucleotide phosphates and switch regions I-III that undergo structural rearrangements when binding different nucleotides. The $G\alpha$ subunit contains 35-93% sequence identity within the four classes.

Guanine Nucleotide-Exchange Factors (GEFs): Surface-cell receptors located within the cell membrane function as signal transducers to the inside of cell by acting as G protein GEFs when stimulated by an agonist (Coleman and Sprang 1996; Gether and Kobilka 1998). They bind the GDP-bound G protein heterotrimer at the C-terminus of the alpha subunit which causes an allosteric conformational rearrangement of $G\alpha$ (Gether and Kobilka 1998; Rohrer and Kobilka 1998; Wall, Posner et al. 1998; Hamm 2001; Sprang 2001; Preininger and Hamm 2004; Oldham and Hamm 2007; Rasmussen, DeVree et al. 2011; Van Eps, Preininger et al. 2011). This effectively enhances nucleotide exchange up to 1,000-fold above basal activity.

Activated receptors, however, are not the only proteins that function as GEFs. Resistance to inhibitors of cholinesterase (Ric-8) proteins are ~60KD cytoplasmic regulators of heterotrimeric $G\alpha$ subunits, expressed in animals and other multicellular eukaryotes (Miller, Alfonso et al. 1996; Miller, Emerson et al. 2000; Miller and Rand 2000). Of the two homologs found in fish, amphibians and mammals, Ric-8A acts specifically on the $G\alpha_{i1/2}$, $G\alpha_{12/13}$ and $G\alpha_{1/11}$ classes of $G\alpha$ subunits (Tall, Krumins et al. 2003).

In vitro experiments have demonstrated that Ric-8A acts catalytically as a GEF that accelerates exchange of GDP for GTP 10-15 fold over the intrinsic rate (Tall, Krumins et al. 2003). An intermediate formed in this reaction, the nucleotide-free $G\alpha$:Ric-8A complex, dissociates in the presence of GTP to regenerate free Ric-8A and $G\alpha$ -GTP (see figure 1 for a cartoon of the catalytic cycle). In the absence of GTP, the $G\alpha$:Ric-8A complex is stable, and can be purified by gel filtration (Tall, Krumins et al. 2003; Tall and Gilman 2004; Chan, Gabay et al. 2011). This biochemical activity of Ric-8A is analogous to that of ligand-activated GPCRs that catalyze nucleotide exchange of heterotrimeric G proteins embedded in the plasma membrane of eukaryotic cells. In contrast to GPCRs, Ric-8A does not catalyze nucleotide exchange on G protein heterotrimers (Tall, Krumins et al. 2003).

Predicted to possess an armadillo-repeat tertiary fold, Ric-8A and its homologs are structurally unrelated to members of the GPCR family (Figuerola, Hinrichs et al. 2009). Ric-8A has also been shown to function as a chaperone for $G\alpha$, facilitating its association with cellular endomembranes, and also inhibiting its ubiquitination and degradation (Hampoelz, Hoeller et al. 2005; Gabay, Pinter et al. 2011; Thomas, Briknarova et al. 2011; Hinrichs, Torrejon et al. 2012; Chan, Thomas et al. 2013; Chishiki, Kamakura et al. 2013). In cell lysates, Ric-8A accelerates $G\alpha$ folding, and over-expression or abrogation of Ric-8A respectively, amplifies or impairs the production of functional $G\alpha$ proteins in a variety of cell lines (Chan, Thomas et al. 2013; Tall, Patel et al. 2013). Ric-8A is an essential regulatory component in the process of asymmetric cell division, particularly in the positioning and movements of cellular mitotic spindles (Couwenbergs, Spilker et al. 2004; David, Martin et al. 2005).

The breadth of this dissertation focuses on the structure-dynamics function of $G\alpha i1$ as it interacts with the GEF Ric-8A and guanine nucleotides. We compare the dynamic nature of the nucleotide (both GDP and GTP) and GEF-bound (Ric-8A) states of $G\alpha i1$ from the ns-to-ms time scale using fluorescence-based methodologies.

Structure of G Proteins: The alpha subunit of G protein heterotrimers is responsible for binding and hydrolyzing guanine nucleotides (Coleman, Berghuis et al. 1994; Coleman, Lee et al. 1994; Wall, Coleman et al. 1995; Coleman and Sprang 1998). It is composed of two domains: a Ras-like and a helical domain. The Ras-like domain is a catalytically functional GTPase and the Helical domain acts as a lid that caps and secures the nucleotide in the binding pocket even though there are not many contact points between the Helical domain and the nucleotide. The Ras-like domain contains signature structural features that regulate catalytic activity through interactions with a variety of binding species (Sprang 1997; Sprang 1997; Sprang 1997; Tesmer, Berman et al. 1997). The switch regions I-III undergo significant structural rearrangements in the transition from GDP-to-GTP bound states (Coleman, Lee et al. 1994). The P-loop is a characteristic of many Ras phosphate coordinating enzymes (Sprang 1997). The C-terminus, the binding site of both receptor and non-receptor GEFs, along with the $\alpha 5$ helix leading to the C-terminus and the $\alpha N/\beta 1$ hinge connecting the two domains are all crucial in nucleotide exchange and GEF activity (Deupi and Kobilka 2007; Kobilka 2007; Oldham and Hamm 2007; Oldham and Hamm 2008; Thomas, Tall et al. 2008; Rasmussen, DeVree et al. 2011; Thomas, Briknarova et al. 2011). Figure 2 is G $\alpha i 1$ bound to GTP γ S and Mg²⁺ with areas of structural interest highlighted. A systematic language has been adopted to describe secondary structure for specific α -helices and β -sheets within the alpha subunit of G proteins. In the Helical domain, α -helices are lettered a-f. In the Ras-like domain, the helices are numbered 1-5 and the β -sheets are numbered 1-6 from N-to-C terminus.

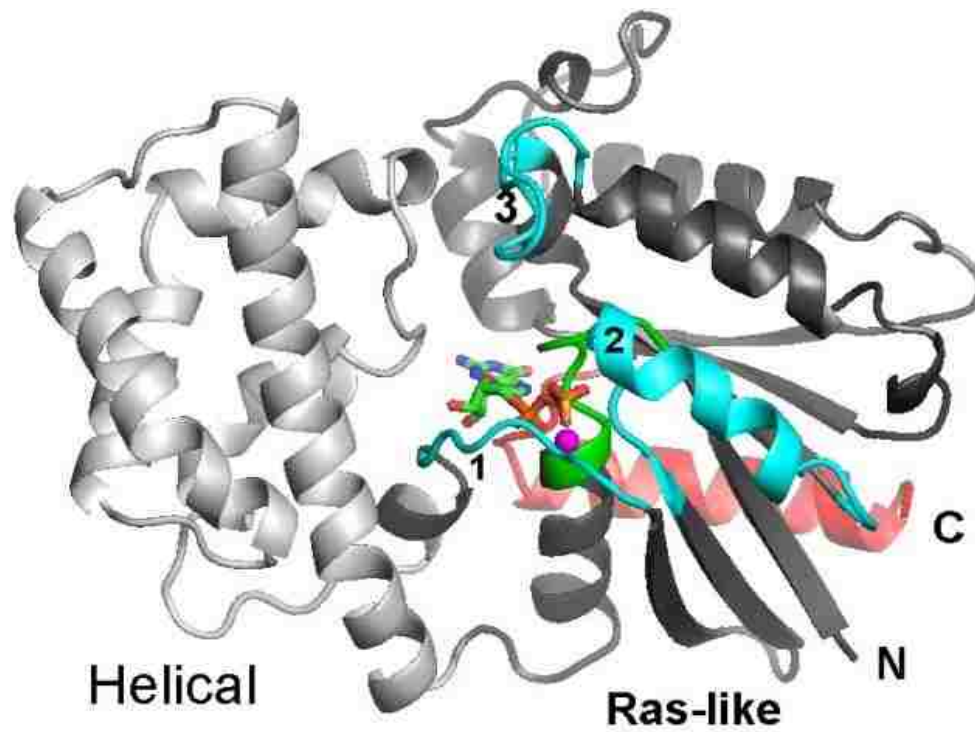


Figure 2 Schematic of the tertiary structure of Gai1, composed of helical (left) and Ras-like (right) domains. Switch segments colored cyan and numbered. The P-loop is colored green, and the amino-terminal (N) and carboxyl-terminal (C) visible in the structure are labeled. The C-terminus, $\alpha 5$ helix, which engages both GPCRs and Ric-8a, is colored pink. GTP is shown as a stick diagram at its inter-domain binding site.

G Protein Dynamics: Crystal structures indicate more structural uniformity in the GTP-bound state compared to the GDP-bound state in G α i1. However, solution-based experiments show G proteins are significantly more dynamic than a rigid crystal. The amino terminus is dynamic in the GDP and GTP-bound states but more well-ordered in the G $\beta\gamma$ and receptor-bound forms (Medkova, Preininger et al. 2002). However, myristoylation of the amino terminus induces more rigidity in nucleotide-, G $\beta\gamma$ - and GPCR-bound states (Preininger, Van Eps et al. 2003). Switch I undergoes dynamic conformational changes consistent with crystal structures with the GDP-bound state more conformationally heterogeneous than GTP-bound (Oldham, Van Eps et al. 2007). Switch II is conformationally labile in the GDP-bound state and binding of G $\beta\gamma$ induces conformational restriction in switch II and α 4, a putative effector binding site. Upon addition of GTP, switch II adopts a unique conformation similar to that of crystal structures but with a flexible backbone (Van Eps, Oldham et al. 2006; Hamm, Meier et al. 2009), indicating a region with significant conformational flexibility despite crystal structures showing a well ordered region. However, the G α subunit can be more conformationally dynamic in the GTP-bound state than in the GDP-bound heterotrimer when nucleotide exchange is induced by a receptor (Ridge, Abdulaev et al. 2006) possibly a mechanism for subunit dissociation. Interestingly, the nucleotide-free state is much more conformationally labile than nucleotide- and GEF-bound states (Thomas, Briknarova et al. 2011).

With respect to the nucleotide binding pocket, mutations in the β 6- α 5 loop leading to the C-terminal result in a steric distortion that influences nucleotide exchange rates (Posner, Mixon et al. 1998; Marin, Krishna et al. 2001; Natochin, Moussaif et al. 2001; Marin, Krishna et al. 2002). The nucleotide binding pocket is destabilized through binding of the C-terminus and conformational changes are allosterically transmitted through α 5 (Nanoff, Koppensteiner et al. 2006; Preininger, Funk et al. 2009). A transient allosteric alteration of switch I is also induced through α 5 (Kapoor, Menon et al. 2009) that destabilizes the phosphate binding motifs (Alexander, Preininger et al. 2014; Kaya, Lokits et

al. 2014). Binding of the C-terminus by a GEF induces a domain opening of the Ras-to-helical allowing solvent accessibility to the nucleotide binding pocket and facilitates nucleotide exchange (Rasmussen, DeVree et al. 2011; Van Eps, Preininger et al. 2011; Van Eps, Thomas et al. 2015).

Ric-8: was discovered through genetic screening of *Caenorhabditis elegans* mutants that are resistant to inhibitors of cholinesterase (Miller, Alfonso et al. 1996). In 2000 Miller *et al.*, showed Go and Gq regulators of neurotransmitter secretion in *C. elegans* function up stream or in conjunction with Ric-8 (Miller, Emerson et al. 2000) and potentiate Gq-mediated signal transduction by acting as a regulator in cells (Nishimura, Okamoto et al. 2006). Ric-8A and Ric-8B (the 2 isoforms) function as GEFs for G α _q, I, o and G α _s, respectively (Tall, Krumins et al. 2003). Ric-8 also acts on G α when it is bound to AGS and RGS proteins (Thomas, Tall et al. 2008; Vellano, Maher et al. 2011).

Reduction of Ric-8 results in embryonic lethality (Miller and Rand 2000; Tonissoo, Lulla et al. 2010). During early development of mice Ric-8 is expressed in the nervous system including the cranial ganglia, neural tube, sympathetic chain and dorsal root ganglia and is also found in the lens, vomeronasal organ, and endolymphatic sac. In the adult brain, it is expressed in the neocortex, hippocampus, and cerebellum as well as in the pineal gland and ependymal layer (Tonissoo, Meier et al. 2003). Ric-8 has also been shown to play a role in regulating spindle positioning in early embryonic development (Afshar, Willard et al. 2004; Couwenbergs, Spilker et al. 2004; David, Martin et al. 2005; Hampoelz, Hoeller et al. 2005; Woodard, Huang et al. 2010). Ric-8A is essential for the enhanced Bergmann glia-basement membrane adhesion required for fissure formation (Ma, Kwon et al. 2012). Its expression is post-transcriptionally controlled during the cell cycle reaching its maximum levels at mitosis (Boullaran, Kamenyeva et al. 2014).

Ric-8B plays a critical role in the control of G α _s protein levels by modulating G α _s ubiquitination and positively regulates Gs signaling (Nagai, Nishimura et al. 2010). Co-expression of Ric-8B effectively

canceled the Gαq-induced ubiquitination of Gαs and recovers cAMP accumulation (Jenie, Nishimura et al. 2013). Ric-8A stabilizes Gαi2 and Gαq by preventing their ubiquitination (Chishiki, Kamakura et al. 2013).

Ric-8 has been shown to play a role in protein transportation and localization. It is required for cortical localization (Afshar, Willard et al. 2005) and Ric-8A levels are critical for the migration of cranial neural crest cells and their subsequent differentiation into craniofacial cartilage during *Xenopus* development (Fuentealba, Toro-Tapia et al. 2013). It is possible that the molecular chaperoning function of Ric-8 is to participate in the folding of nascent Gα subunits (Chan, Thomas et al. 2013; Tall 2013). Ric-8 folding of G proteins may better explain the apparent amplification of G protein-coupled receptor signaling (Chan, Thomas et al. 2013; Tall 2013).

Ric-8 is approximately 80% α-helix, consistent with an armadillo repeat-type structure (Figuroa, Hinrichs et al. 2009). It stabilizes a conformationally dynamic nucleotide-free Gα, and may act in a manner similar to a GPCR in that it binds at the C-terminus (Thomas, Briknarova et al. 2011). It induces a conformationally heterogeneous state of Gαi1, an insight into the mechanism of action for a non-receptor Gα GEF's (Van Eps, Thomas et al. 2015). However, it remains unresolved whether, in cells, Ric-8A regulates the GTPase cycle of Gα subunits in its capacity as a GEF or whether its GEF activity is simply a byproduct of its role as a chaperone needed to maintain a sufficient pool of functional protein.

Dissertation Aims: The wealth of structural knowledge of G proteins has given extensive insight into the mechanism and function of the signaling enzyme. Work on the Gαi1/s subunit involving GPCR's has shown a Helical-to-Ras-like domain separation is necessary for enhanced nucleotide exchange. The Helical domain must be displaced up to 40 Å from the Ras-like domain to expose the nucleotide binding pocket to solvent (Rasmussen, DeVree et al. 2011; Van Eps, Preinerger et al. 2011). Dynamic studies of

this event using fluorescence and EPR methods have shown secondary structural elements participating in conformational changes and estimates the time-scales of the secondary structural dynamics involved. However, there have only been a few investigations involving the dynamics of G α interacting with Ric-8A (Thomas, Briknarova et al. 2011) . Studies involving the structural changes of G α binding to Ric-8A show some similarities with GPCR's (Van Eps, Thomas et al. 2015). Conformational changes and secondary structure time-scales were resolved using DEER and EPR spectroscopy and low-resolution conformational dynamics information was extracted using X/D exchange MS (Thomas, Briknarova et al. 2011). However, a void still exists in determining the time-scales for the structural dynamics of G protein binding to Ric-8A and presents an opportunity for fundamental scientific discovery. **Hypothesis statement: It is hypothesized that GEF binding induces a molten-globule like state within G α able to rapidly exchange nucleotide by altering segmental motions and conformational dynamics.** These altered dynamics allow G α to “pre-organize” into low probability states that otherwise would not be accessible. To test this hypothesis, two specific aims have been developed.

The aims of the dissertation are: 1) To resolve the time-scales for the dynamics involved in G protein secondary-structural segmental motion in the nucleotide (GDP/GTP-bound) and GEF-bound (Ric-8A-bound) states using time-resolved fluorescence anisotropy. 2) To determine the conformational change rates of inter and intra-domain double-mutant freely diffusing G α i1, bound to GDP, GTP or in the complex with Ric-8A. The conformational change rates were extracted from the distributions of smFRET efficiencies at varying binning times using the 3-Gaussian method (Gopich and Szabo 2010; Chung, Gopich et al. 2011). This method informs on the number of structural states and the kinetics of the associated conformational equilibria.

Chapter 2

Segmental Dynamics of $G\alpha$

Introduction

Heterotrimeric G proteins relay signals received at the surface of cells by interacting with activated (agonist-bound) 7-transmembrane, G-protein-coupled receptors (GPCRs). The alpha subunit of the G Protein $\alpha\beta\gamma$ heterotrimer, $G\alpha$, binds guanine nucleotides and regulates signaling through the hydrolysis of GTP to GDP (Coleman, Berghuis et al. 1994; Coleman, Lee et al. 1994; Raw, Coleman et al. 1997). When GTP is bound, $G\alpha$ is in the “on” state and signaling is activated. After hydrolysis, when GDP is bound, $G\alpha$ is in the “off” state and signaling is quenched. Reactivation of $G\alpha$ requires release of GDP and exchange for GTP. This nucleotide exchange process, which is the rate-limiting step for GTP hydrolysis by the GTPase, is catalyzed by activated GPCRs. Activated GPCRs, and other proteins known to catalyze exchange of GDP for GTP, are known as guanine-exchange factors (GEFs). In our experiments, we probe the dynamics of $G\alpha$ while bound to the GEF Resistance to Inhibitors of Cholinesterase-8A (Ric-8A) (Miller, Alfonso et al. 1996; Miller, Emerson et al. 2000; Miller and Rand 2000; Tall, Krumins et al. 2003). Ric-8A is a soluble 60-kDa protein located in the cytosol that has been shown to have GEF activity for a variety of $G\alpha$ subunits, increasing the rate of nucleotide exchange up to 15 times (Miller and Rand 2000; Tall, Krumins et al. 2003). Although Ric-8A has GEF activity, it is not known whether it functions in down-stream signaling. It is not a member of the receptor class of regulators of G protein signaling, but appears to have a crucial role in asymmetric cell division.

Much has been learned about the mechanism of G-protein nucleotide exchange from crystal structures and DEER spectroscopy studies (Sprang 1997; Chung, Rasmussen et al. 2011; Van Eps, Preininger et al. 2011; Van Eps, Thomas et al. 2015). A structure of the $G\alpha i1$ is shown in Figure 2. This GTPase is composed of two domains: the Ras-like and the Helical domain. The Ras-like domain structurally resembles other small GTPases and hydrolyses GTP in a similar manner. The Helical domain acts as a “lid”, which caps and secures the guanine nucleotide in its binding pocket, which is wedged between the two domains. Kobilka, *et. al.* crystalized the $G\alpha\beta\gamma$ heterotrimer bound to an activated

receptor and observed a large Helical-Ras-like domain-domain separation occurs when the complex is formed (Rasmussen, DeVree et al. 2011) and allosteric perturbations of the switch regions, I and II, transmitted through $\alpha 5$ results from GPCR binding at the C-terminus (Oldham, Van Eps et al. 2007; Preininger, Parello et al. 2008). However, there is limited dynamic information, crucial to our understanding of G protein function (i.e., the mechanism of nucleotide exchange), about $G\alpha$ when it is bound to a GEF. Electron density in the switch regions II and III are missing while switch I undergoes significant structural changes from the GTP to GDP-bound form, implying conformational heterogeneity within the structures. DEER spectra of the nucleotide and GEF-bound (Ric-8A and GPCRs) form also show a heterogeneous molten-globule like state that has multiple conformational states and considerably greater spectral peak widths, alluding to greater flexibility within those states when GEF-bound (Van Eps, Preininger et al. 2011; Van Eps, Thomas et al. 2015). This raises the question, what are the dynamics involved in these conformational changes and how does a GEF affect these states?

The aim of the present investigation is to resolve the time-scales for the dynamics involved in G protein secondary-structure segmental motion between the GDP, GEF (Ric-8A bound) and GTP-bound states using time-resolve fluorescence anisotropy.

Methods

Protein Expression and Purification: A plasmid encoding $G\alpha i 1$ that contained six amino acid substitutions at solvent-exposed cysteine residues (C3S-C66A-C214S-C305S-C325A-C351I) and a hexahistidine tag between amino acid residues M119 and T120 (HEXA 1) was inserted into the vector pDest 15, containing a Lac (Isopropyl β -D-1-thiogalactopyranoside (IPTG) inducible) promoter for expression and glutathione-s-transferase (GST)- *Tobacco Etch Virus* (TEV) protease digestion site for affinity purification (Medkova, Preininger et al. 2002). Site-directed mutagenesis using the QuickChange

II Site-Directed Mutagenesis Kit (Invitrogen) was used to exchange select residues (E63C, Q106C, K180C, K209C, E238C, 305C and K330C) with cysteine in the HEXA 1 background. The plasmids containing HEXA 1 and the residue mutations were transformed into BL21 DE3 competent cells. Fresh colonies of transformed cells were picked and inoculated into 100 mg L⁻¹ ampicillin-Luria-Bertani (LB) media (1 L @ 37 °C) and grown until OD₆₀₀ reached 0.6. The temperature of the culture was reduced to 19°C and expression was induced with IPTG. Cells were grown for 16 hours, pelleted, then stored at -80 °C. Cells were harvested by suspending them in lysate buffer Gai1 (50 mM Tris pH 8.0, 150 mM NaCl, 10% glycerol, 2 mM dithiothreitol (DTT), 2 mM phenylmethanesulfonyl fluoride (PMSF), 100 uM GDP) (5 mL g⁻¹ cells) and then lysed by sonicating on ice for 5 minutes. The cell lysate was centrifuged at 13,000 g for 30 minutes, at which point it was passed over glutathione-sepharose beads (Invitrogen) and washed extensively with lysate buffer Gai1. TEV protease was then added (1:10 ratio TEV to protein) and cleaved the sample for 16 hours at 4 °C. The cleaved protein sample was eluted with Q-A buffer (50 mM Tris pH 8.0, 2 mM DTT). Further purification was by ion-exchange chromatography on a Q column. The protein sample was eluted using a 0-1 M NaCl gradient at a flow rate of 2 ml/minute, fractions containing sample were pooled, and the final purity was estimated at greater than 95 percent, based on SDS-PAGE electrophoresis.

A plasmid containing a truncated mammalian Ric-8A (1-491) construct with a lac promoter for induction (IPTG) and a hexahistidine affinity tag was transformed into BL21 DE3 competent cells. Fresh colonies were picked and placed into 1 L cultures of LB media with 50 mg L⁻¹ kanamycin at 37 °C. Cultures were allowed to grow until OD₆₀₀ reached 0.6. The culture temperature was reduced to 19 °C, induced with IPTG and allowed to grow for 16 hours. Induced cells were collected, pelleted and stored at -80 °C. Mammalian Ric-8A (1-491) containing cells were suspended into lysis buffer Ric (50 mM Tris pH 8.0, 250 mM NaCl, 2 mM PMSF, 1 mM imidazole) and lysed by sonication on ice for 5 minutes. The cell lysate was then spun down at 13,000 g and the supernatant was passed over a Ni²⁺ immobilized

metal ion affinity column (IMAC) resin. The column was washed extensively with wash buffer Ric (50 mM Tris pH 8.0, 250 mM NaCl, 10 mM imidazole) and eluted with elution buffer (50 mM Tris pH 8.0, 250 mM NaCl, 250 mM imidazole). The eluted sample was dialyzed in Q-A buffer to remove excess salt and imidazole and then subjected to ion-exchange chromatography on a Q column. The sample was eluted with a 0-1M NaCl gradient, the fractions containing sample were pooled, and the final purity was estimated to be 90-95% based on SDS-PAGE electrophoresis.

Protein Fluorescence Labeling: Mutant Gai1 HEXA 1 samples (E63C, Q106C, K180C, K209C, E238C, C/S305C and K330C) were reduced in 10 mM DTT for 30 minutes (50 mM Tris pH 8.0, 250 mM NaCl, 100 μ M GDP, 10 mM DTT) and buffer exchanged using Millipore Amicon Ultra concentrator centrifuge tubes (30 kDa cutoff) to labeling buffer (20 mM MOPS pH 7.4, 250 mM NaCl, 100 μ M GDP, 10% glycerol). 100-200 μ L of a 100- μ M reduced protein sample was allowed to react with equimolar Alexa 488 (C5) maleimide (1:1 ratio protein, 100-200 nmol Alexa (C5) 488 maleimide label from stock aliquots where methanol solvent was removed under vacuum) for 15 minutes. The reaction was quenched with the addition of β -mercaptoethanol (β -ME) to a final concentration of 10 mM and passed over a 10 mL G 10 desalting column (Invitrogen) to remove unreacted dye, and then passed through a 0.22- μ m filter to remove aggregated protein. All labeled protein was subjected to mass spectrometry to ensure non-specific labeling was not present (appendix).

Gai1 Functional Assays: Functional assays were developed to ensure labeled Gai1 samples were competent to (1) bind Ric-8A and exchange nucleotide from GDP to GTP and (2) determine the rate at which nucleotide is exchanged. (1) Nucleotide exchange assay: freshly labeled Gai1 samples were diluted to 1 μ M in 20 mM Hepes pH 8.0, 100 mM NaCl, 2 mM DTT, 0.01% C12E10 with either 100 μ M GDP, 1.5 μ M Ric-8A or 1.5 μ M Ric-8A+10 μ M GTPyS+10 mM Mg²⁺ for each binding state, respectively, and the mixture was allowed to rest on ice for 30 minutes. Each sample was passed over a Superdex S200 (GE) size-exclusion column at a flow rate of 0.4 mL/min and monitored at 280 nm using an Acta

series 1200 FPLC resulting in separating free-Gai1 from the Ric-8A-bound species. (2) Intrinsic tryptophan fluorescence assay: Freshly prepared Gai1 (both labeled and unlabeled) were diluted to 1 μM in 20 mM HEPES pH 8.0, 100 mM NaCl, 10 mM Mg^{2+} , 0.05% C12E10 with 0 or 1.5 μM Ric-8A present. GTP γ S was added to the sample at a final concentration of 10 μM to initiate the reaction. The reaction was monitored by emission at 340 nm after excitation at 295 nm (10-nm bandpass excitation and emission) continuously for 20 min using a Perkin-Elmer LS 55 luminescence fluorimeter. Three individual data sets for each sample were globally fit to a single exponential function to determine the rate using the program OriginPro 9.0.

For time-resolved fluorescence anisotropy analysis, 1- μM labeled Gai1 samples in assay buffer (20 mM HEPES pH 8.0, 100 mM NaCl, 2 mM DTT, 0.05% C12E10) containing either 100 μM GDP, 1.5 μM Ric-8A or 1.5 μM Ric-8A+10 μM GTP γ S+10 mM Mg^{2+} , were passed over a Superdex S200 (GE) size-exclusion column using FPLC (Acta series 1200), monitoring at 280 nm identifying free Gai1 sample and/or sample bound to Ric-8A. Samples with fractions corresponding to 40 kDa (15.2 mL elution volume, GDP and GTP γ S-bound) or 95 kDa (12.5 mL elution volume, Ric-8A-bound) kDa were pooled and used for data acquisition.

Experimental Setup and Data Collection: Single-molecule measurements were carried out using an inverted-confocal Olympus Fluoview IX71 microscope fitted with a 60X 1.2-numerical aperture (NA) water-objective. A 470-nm pulsed-diode laser (30 μW , PicoQuant Model LDH-P-C-470) was used for excitation and avalanche photodiodes (Perkin-Elmer Optoelectronic photo-counting module model SPCM-AQR-14-FC) were used for emission detection. Emission was routed into a detection channel using a 535/50-nm bandpass filter. The Alexa (C5) 488 β -ME adduct was used to calibrate the confocal optical train with a molecular brightness (β) of 140 ± 20 counts $\text{molec}^{-1} \text{s}^{-1} \text{uW}^{-1}$ and known translational diffusion coefficient of $420 \pm 5 \mu\text{m}^2 \text{s}^{-1}$ (Dertinger, Loman et al. 2008; Muller, Weiss et al. 2008).

Alexa488-labeled Gai1 samples were diluted to 100-500 pM in a background of single-molecule buffer

(20 mM HEPES pH 8.0, 100 mM NaCl, 2 mM DTT, 0.05% C12E10) with either 100 μ M GDP, 1 μ M Ric-8A, or 10 μ M GTP γ S + 10 mM Mg²⁺ for each respective G α i1 binding state. Typical data collection time was 15 minutes, yielding at least 10,000 photon counts at the peak maximum of the time-resolved emission decay curve. SymPhoTime v5.3.2.2 (PicoQuant) was used for data acquisition and analysis for extraction of the translational diffusion coefficients.

Fluorescence lifetime and time-resolved anisotropy measurements were carried out by time-correlated single-photon counting (TCSPC), using the FLASC 1000 sample chamber (Quantum Northwest, Liberty Lake, WA), which has a unique T format for simultaneous detection of horizontal (H), vertical (V) and variable polarization components of the emission. FLASC 1000, fitted with a temperature controlled cuvette chamber (TC 125, Quantum Northwest), used a 470-nm pulsed- LDH-P-C 470 laser diode (10 MHz, PicoQuant) for excitation (magic angle, 54.7° and vertical) and photon detection module (IBH model TBX-04) with 525/50 nm (Chroma) filters were used for emission detection in the vertical and horizontal planes using a beam-splitting Glan-Thompson polarizer (Karl Lambrecht) separating the H and V components. This optical arrangement allows simultaneous detection of up to three polarization components of the emission—typically H, V and magic angle—by separate photomultipliers, which assures collection of decay curves under identical excitation conditions. The V and H decay curves, which contain the information about dynamics, were collected for equal lengths of time, using the TimeHarp 200 PCI board (PicoQuant, Berlin), until 4×10^4 counts were obtained at the maximum of the V curve with a timing resolution of 35 ps/channel.

The time-resolved anisotropy, $r(t)$, is given by

$$r(t) = \frac{I_{VV}(t) - I_{VH}(t)}{I_{VV}(t) + 2I_{VH}(t)} \quad (1)$$

where $I_{VV}(t)$ and $I_{VH}(t)$ represent the vertical and horizontal decays, respectively, obtained using vertical excitation. The denominator of Eq. 1 is the total intensity decay, $I(t)$.

If there is segmental motion in a region of the protein containing the probe, there will be additional depolarization of the fluorescence, which will produce a correlation time in the anisotropy decay, $\phi_{segmental}$, which is shorter than ϕ_{global} , the rotational correlation time of the entire protein. In this case, the appropriate equation for the anisotropy decay is

$$r(t) = r_0 \left[\gamma e^{\frac{-t}{\phi_{segmental}}} + (1 - \gamma) e^{\frac{-t}{\phi_{global}}} \right] \quad (2)$$

where γ is a weighting factor between 0 and 1. Because anisotropy decay data are typically fit as a sum of exponentials, when there is segmental motion, the decay law becomes

$$r(t) = r_0 [p_{short} e^{\frac{-t}{\phi_{short}}} + p_{long} e^{\frac{-t}{\phi_{long}}}] \quad (3)$$

where $p_{short} = \gamma$ and $p_{long} = 1 - \gamma$. Also, $r_0 \times p_{short} = \beta_{segmental}$ and $r_0 \times p_{long} = \beta_{global}$. Accordingly,

$$\phi_{short}^{-1} = \phi_{segmental}^{-1} + \phi_{global}^{-1}; \quad \phi_{long}^{-1} = \phi_{global}^{-1}. \quad (4)$$

The individual vertical and horizontal decay curves, $I_{VV}(t)$ and $I_{VH}(t)$, respectively, were fit simultaneously, using the analysis software package FluoFit Pro v4.6.6.0 (PicoQuant, Berlin) to extract the fitting parameters $\phi_{segmental}$, $\beta_{segmental}$, and ϕ_{global} , β_{global} . The sum of $\beta_{segmental}$ and β_{global} is the zero-time, anisotropy r_0 .

Fluorescence Correlation Spectroscopy: Fluorescence fluctuations in time, $\partial F(t) \equiv F(t) - \langle F(t) \rangle$, can be induced by a variety of processes and depend on various photophysical parameters (Lakowicz 2006).

Following the treatment of Schwille *et al.*, the normalized fluorescence fluctuation autocorrelation

function $G_{ii}(\tau)$ with lag time τ is defined as (Medina and Schwille 2002; Bacia and Schwille 2007; Ries and Schwille 2012; Bacia, Haustein et al. 2014);

$$G_{ii}(\tau) = \left\langle \frac{\partial F_i(t) \partial F_i(t + \tau)}{F_i(t)} \right\rangle^2 \quad (5)$$

Assuming the fluctuations are due to changes in concentration (so-called number fluctuations), they can be described by a normalized three-dimensional (3D) diffusion autocorrelation function for species i :

$$G_{ii}(\tau) = \sum_{i=1}^n \rho_i \left(1 + \frac{\tau}{\tau_i}\right)^{-1} \left(1 + \frac{\tau}{\tau_i \kappa^2}\right)^{-\frac{1}{2}}. \quad (6)$$

$\sum_{i=1}^n \rho_i = \frac{1}{\langle N \rangle}$ is the inverse of the average number of molecules inside the effective measurement

volume, $V_{eff} = \pi^{\frac{2}{3}} \omega_0^2 Z_0$, and $\tau_i = \frac{\omega_0^2}{4D_i}$ is defined as the average lateral diffusion time for a molecule of

species i , through V_{eff} . The ellipticity of V_{eff} is defined as $\kappa = \frac{Z_0}{\omega_0}$ the ratio of vertical to horizontal radii.

Thus, an unknown diffusion coefficient can be easily derived from the characteristic decay time, τ_i , when

V_{eff} is properly calibrated with a known standard. However, the shape of $G_{ii}(\tau)$ can be significantly

distorted by singlet-to-triplet state conversions of the excited state dye, which is independent of

calibration, that are on the same timescale as diffusion. To account for this perturbation, a “triplet”

state character τ_T , is input into $G_{ii}(\tau)$:

$$G_{ii}(\tau) = (1 - T + T e^{-\frac{\tau}{\tau_T}}) \sum_{i=1}^n \rho_i \left(1 + \frac{\tau}{\tau_i}\right)^{-1} \left(1 + \frac{\tau}{\tau_i \kappa^2}\right)^{-\frac{1}{2}} \quad (7)$$

and $\sum_{i=1}^n \rho_i = \frac{1}{\langle N \rangle (1-T)}$.

Error Analysis: The error in parameters recovered from the anisotropy and FCS data was calculated at the 95% confidence limit by using the Support-Plane method (Grams, Johnson et al. 1972), available in the software packages FluoFit (v4.6.6.0) and SymphoTime (v5.3.2.2, PicoQuant, Inc.)

Results

Gai1 Activity Assays of labeled protein: Superdex S200 size exclusion yielded binding states for free labeled Gai1 (15.2 mL elution volume) and Ric-8A bound species (12.5 mL elution volume) and demonstrated that labeled-Gai1 can bind Ric-8A (98% binding, N=7) and exchange nucleotide (GDP for GTP γ S, 95% nucleotide exchange N=7). The increase of Intrinsic tryptophan fluorescence, monitored after the addition of GTP γ S, demonstrated that all Gai1 samples bind GTP γ S, without and with Ric-8A present, at a rate of 0.02 ± 0.01 and $0.3 \pm 0.2 \text{ min}^{-1}$ respectively (N = 7 without and N = 14 with Ric-8A).

Fluorescence Anisotropy and Fluorescence Correlation Spectroscopy: To assess the secondary structural dynamics of key elements within Gai1 when bound to nucleotide or the GEF Ric-8A, time-resolved fluorescence anisotropy was employed. Seven cysteine mutations were introduced into the surface-cysteine-free construct Gai1 HEXA 1. These mutations were E63C (connecting the Helical to Ras domains), Q106C (α -c of the helical domain), K180C (switch I), K209C (switch II), E238C (switch III), 305C (α 4 of the Ras domain) and K330C (α 5) leading to the C-terminus in the Ras domain).

In principle, the time-resolved anisotropy is most sensitive to rotational correlation times close to the excited-state lifetime (Brochon, Wahl et al. 1977). However, in practice, the uncertainty in recovered rotational correlation times increases significantly when these times exceed five-fold the probe's excited-state lifetime (Minazzo, Darlington et al. 2009). For example, using the Stokes-Einstein and Stoke-Einstein-Debye relations and assuming prolate ellipsoids with axial ratios from 1:1 to 1:3 (Small and Isenberg 1977) for Gai1 with a molecular weight of 41 KDa, at 23°C, the calculated global

rotational correlation time (ϕ_{global}) is 14-17 ns. Because the average fluorescence lifetime (τ) of Alexa 488 is about 4 ns, the ratio of ϕ_{global} to τ is at most 4:1. Being less than 5:1, this ratio is marginally suitable for determination of the global correlation time. However, when G α i1 HEXA 1 is bound to Ric-8A, the calculated global rotational time of the complex is 45-55 ns, and the ϕ_{global} to τ ratio for the complex will be close to 13:1. Because the global correlation times are much longer than the average lifetime of the fluorescent probe, and because there is cross-correlation between the anisotropy parameters, recovering accurate values for the amplitudes and correlation times of the global and segmental motions is difficult. To reduce the cross-correlation and uncertainty in the global rotational parameters, we used independent information from translational diffusion of the proteins and their Ric-8A complexes obtained by FCS.

Translational and rotational diffusion are related by the Stokes-Einstein and Stokes-Einstein-Debye relations, and the global rotational correlation time can be calculated from the translational diffusion coefficient (Ries and Schwille 2012). Accordingly, the global correlation times for the G α i1 complexes were calculated from the FCS-determined translational diffusion coefficients and then input as fixed values in the analysis of the anisotropy decay data.

Gαi1 Mutant	D_{Translational} (μm² s⁻¹)		
	GDP	Ric-8A	GTPγS
E63C	92 (-6, 7)	72 (-7, 8)	95 (-4, 5)
Q106C	93 (-4, 4)	56 (-5, 7)	85 (-6, 7)
K180C	92 (-6, 7)	69 (-4, 5)	97 (-7, 8)
K209C	100 (-16, 19)	58 (-6, 7)	86 (-7, 8)
E238C	108 (-7, 8)	77 (-7, 8)	93 (-4, 5)
305C	105 (-9, 10)	50 (-4, 5)	93 (-10, 12)
K330C	93 (-5, 6)	71 (-3, 3)	99 (-5, 6)
Average	97 (-7, 9)	65 (-5, 6)	92 (-6, 7)

Table 1 Translational diffusion coefficients of Gαi1 in the presence of saturating concentrations of nucleotide (GDP, GTPγS) or GEF (Ric-8A) (Tall, Krumin et al. 2003) determined by fluorescence correlation spectroscopy at 21 °C. Brackets represent uncertainty at the 95% confidence limits determined by using the support-plan method (Grams, Johnson et al. 1972).

Table 1 lists the diffusion coefficients of Gai1 mutants extracted using eq.7. Gai1 under nucleotide saturating conditions (GDP and GTPγS) had similar diffusion coefficients of $97 \pm (-6, 7) \mu\text{m}^2 \text{s}^{-1}$ and $92 \pm (-5, 6) \mu\text{m}^2 \text{s}^{-1}$ and the GEF bound state (Ric-8A) had a slower diffusion coefficient of $65 \pm (-5, 6) \mu\text{m}^2 \text{s}^{-1}$. These values translate to global-rotational correlation times of 15 (-1, 2) ns and 53 (-4, 4) ns for nucleotide and Ric-8A bound states. Fixing the global correlation times recovered from FCS data reduces the cross-correlation between the fitted amplitudes (β_i -factor) and the segmental rotational correlation time ($\phi_{\text{segmental}}$). Table 2 and figure 3 are the segmental correlation times ($\phi_{\text{segmental}}$ see eq. 4) and fraction $\beta_{\text{segmental}}$ contribution for each Gai1 mutant in their binding state (nucleotide and GEF).

“Wobble-in-a-cone” Model: To better understand the contribution of the segmental motions to the anisotropy decay of Gai1, we employed the wobble-in-a-cone model (square-well potential) (Kinosita, Ikegami et al. 1982). This model assumes that the fraction $\beta_{\text{segmental}}$ compared to β_{global} reflects spatial limits for the local motions of the probe (i.e., smaller cone angles imply greater local restriction and, conversely, larger cone angles imply greater range of motion). Recall that the sum of $\beta_{\text{segmental}}$ and β_{global} is the limiting anisotropy at zero time, r_0 . In the wobbling-cone model, the angle θ with respect to the symmetry axis of the cone can be estimated using the relationship

$$\frac{\beta_{\text{global}}}{r_0} = \left[\frac{1}{2} \cos \theta (1 + \cos \theta) \right]^2 . \quad (8)$$

Table 2 and Figure 3 show the cone angles for the various Gai1 mutants in their binding states.

Gai1 Mutant- GDP	Cone Angle θ		Φ_{Global} (ns)	$\Phi_{\text{Segmental}}$ (ns)	$\langle r \rangle$	r_0	χ^2
	$\beta_{\text{segmental}} / \Sigma \beta_i$	($^\circ$)					
E63C	0.44 (-0.04, 0.04)	35 (-2, 2)	15 (-1, 2)	1.2 (-0.2, 0.3)	0.142	0.2533	1.166
Q106C	0.53 (-0.04, 0.03)	39 (-2, 2)	15 (-1, 2)	1.7 (-0.3, 0.3)	0.148	0.2617	1.140
K180C	0.12 (-0.03, 0.04)	16 (-2, 3)	15 (-1, 2)	1.3 (-0.5, 0.9)	0.185	0.2555	1.029
K209C	0.16 (-0.03, 0.03)	19 (-2, 2)	15 (-1, 2)	1.6 (-0.5, 0.8)	0.200	0.2784	1.110
E238C	0.22 (-0.03, 0.04)	23 (-2, 2)	15 (-1, 2)	1.3 (-0.2, 0.5)	0.199	0.2908	1.068
305C	0.43 (-0.04, 0.04)	34 (-2, 2)	15 (-1, 2)	1.0 (-0.2, 0.2)	0.159	0.2839	1.156
K330C	0.52 (-0.04, 0.05)	39 (-2, 3)	15 (-1, 2)	1.1 (-0.2, 0.2)	0.122	0.2353	1.130
Ric-8A							
E63C	0.27 (-0.02, 0.02)	26 (-1, 1)	53 (-4, 4)	2.3 (-0.5, 0.7)	0.253	0.3176	1.203
Q106C	0.57 (-0.03, 0.03)	41 (-1, 2)	53 (-4, 4)	2.2 (-0.4, 0.4)	0.177	0.2772	1.165
K180C	0.23 (-0.02, 0.02)	24 (-2, 1)	53 (-4, 4)	2.7 (-0.7, 0.9)	0.262	0.3171	1.128
K209C	0.33 (-0.02, 0.02)	29 (-1, 1)	53 (-4, 4)	2.8 (-0.6, 0.6)	0.247	0.3179	1.215
E238C	0.44 (-0.03, 0.03)	35 (-2, 1)	53 (-4, 4)	1.5 (-0.3, 0.3)	0.181	0.2745	1.148
305C	0.53 (-0.03, 0.03)	40 (-2, 1)	53 (-4, 4)	1.5 (-0.3, 0.3)	0.164	0.2723	1.210
K330C	0.27 (-0.02, 0.02)	26 (-1, 1)	53 (-4, 4)	2.3 (-0.5, 0.6)	0.239	0.3021	1.072
GTPyS							
E63C	0.45 (-0.04, 0.04)	35 (-2, 2)	15 (-1, 2)	1.3 (-0.3, 0.3)	0.139	0.2519	1.149
Q106C	0.52 (-0.03, 0.04)	39 (-2, 2)	15 (-1, 2)	1.7 (-0.3, 0.3)	0.153	0.2689	1.076
K180C	0.30 (-0.03, 0.03)	28 (-2, 1)	15 (-1, 2)	1.8 (-0.4, 0.5)	0.180	0.2796	1.095
K209C	0.33 (-0.04, 0.05)	29 (-2, 2)	15 (-1, 2)	1.0 (-0.2, 0.2)	0.180	0.2865	1.296
E238C	0.25 (-0.03, 0.04)	25 (-2, 2)	15 (-1, 2)	1.2 (-0.3, 0.3)	0.212	0.3259	1.132
305C	0.72 (-0.06, 0.06)	50 (-3, 4)	15 (-1, 2)	1.2 (-0.2, 0.2)	0.088	0.2182	1.189
K330C	0.53 (-0.04, 0.05)	39 (-2, 3)	15 (-1, 2)	1.2 (-0.2, 0.2)	0.117	0.2290	1.135

Table 2 Recovered parameters of globally fixed (Φ_{global}) anisotropy decay curves for Gai1 mutants at 25 °C. The short correlation time, $\Phi_{\text{segmental}}$, and β_i 's were used to explain the dynamic nature of secondary structure for Gai1 in its various binding states (GDP, Ric-8A and GTPyS-bound). The recovered β_i 's partition depolarization into global and segmental components and were used to calculate the degree of depolarization of local secondary structure. Steady-state ($\langle r \rangle$, steady-state anisotropy) and frozen (r_0) anisotropy report on the efficiency of depolarization and the χ^2 value reports on the goodness of the fit. The 95% confidence limits, calculated by the support-plane method (Grams, Johnson et al. 1972), are reported within the parenthesis.

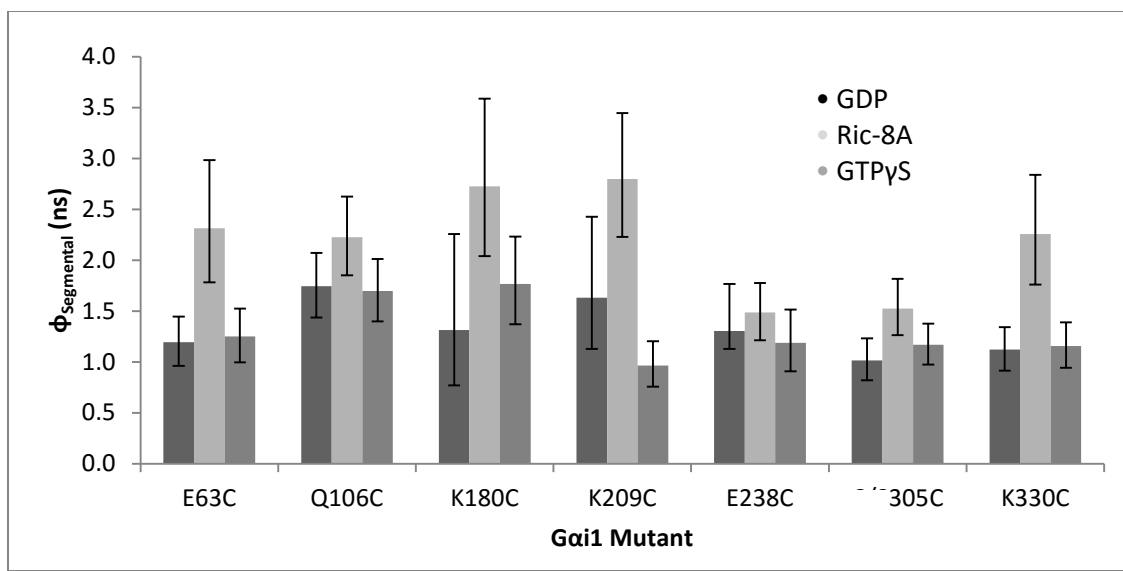


Figure 3 Segmental correlation times reported in Table 2 for each binding state GDP, Ric-8A and GTP with uncertainty at the 95% confidence limits determined using the support-plane method (Grams, Johnson et al. 1972).

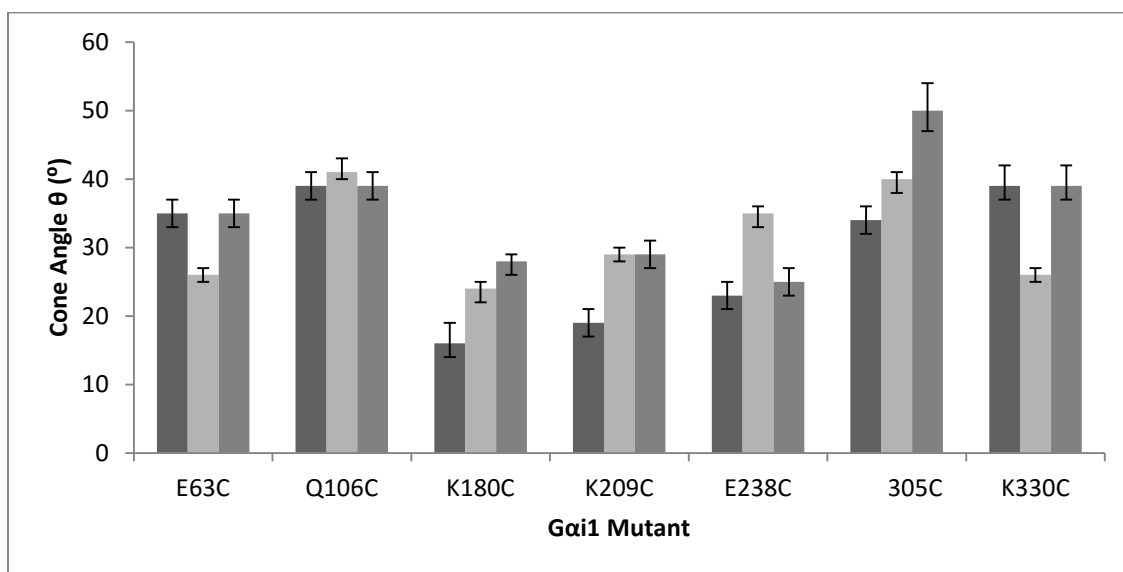


Figure 4 Cone angles reported in Table 2 for each binding state GDP, Ric-8A and GTP with uncertainty at the 95% confidence limits (Grams, Johnson et al. 1972).

Discussion

Two parameters that quantify the extent and rates of depolarization, respectively, are the pre-exponential terms (β_i) and the rotational correlation times (ϕ_i). An *increase* in $\beta_{\text{segmental}}$ relative to β_{global} reflects a *decrease* in structural barriers restricting the volume in which depolarization can occur. These barriers may be described adequately by the wobbling-in-a-cone model (Kinosita, Ikegami et al. 1982) without a detailed structural model. However, the magnitudes of the segmental correlation times do suggest what kinds of motions might be contributing to the depolarization rate. Sub-nanosecond correlation times will be dominated by amino acid side chain dynamics, correlation times of a few nanoseconds may be associated, for example, with loop dynamics, whereas longer segmental rotational correlation times ($\phi_{\text{segmental}}$) may be attributed to increased involvement of additional elements of secondary structure, such as whole helices, sheets or domain motions (Alexiev, Rimke et al. 2003; Bayley, Martin et al. 2003; Schroder, Alexiev et al. 2005; Kim, Schlieter et al. 2012). Without an explicit structural interpretation, the results of the cone-angle analysis and comparison of the relative timescales of the segmental motions provide information about parts of a protein that are either more or less dynamic on the nanosecond timescale. The aim of this study is *not* to assign explicit local dynamic behavior, but instead to compare the dynamic nature of the various binding states of Gai1 and how they may contribute to enzymatic function.

Individual Gai1 Mutant Depolarization Trends by Binding State: In the fitting of the anisotropy decays of the Gai1 mutants, the global (long) rotational correlation times were constrained to 15 and 53 ns for nucleotide and GEF (Ric-8A) bound states, respectively. These correlation times were derived from diffusion coefficients recovered from FCS data. Figures 5 and 6 show the locations for each mutant within Gai1.

Gai1 HEXA 1 E63C has segmental correlation times of 1.2 (-0.2, 0.3), 2.3 (-0.5, 0.7) and 1.3 (-0.3, 0.3) ns and fractions $\beta_{\text{segmental}}$ of 0.44 (-0.04, 0.04), 0.27 (-0.02, 0.02) and 0.45 (-0.04, 0.04) for the GDP, Ric-8A and GTP γ S respectively. The GDP and GTP states have equal $\phi_{\text{segmental}}$ values, about half that of the Ric-8A bound state. The fraction $\beta_{\text{segmental}}$ for the GDP and GTP bound states is 63% larger than that of the Ric-8A bound state. The shorter $\phi_{\text{segmental}}$ and larger fraction $\beta_{\text{segmental}}$ (larger cone angle) of the nucleotide-bound states indicate less local rigidity at position E63C when nucleotides are bound. Conversely, the longer $\phi_{\text{segmental}}$ and smaller fraction $\beta_{\text{segmental}}$ (smaller cone angle) indicate greater local rigidity when Ric-8A is bound. *Gai1 E63C* is located at the hinge region between the Helical and Ras-like domain in helix α B of the Helical domain. Knowing that the Helical and Ras-like domain move apart by as much as 40 Å during GEF-induced nucleotide exchange (Van Eps, Preininger et al. 2011; Shukla, Manglik et al. 2013; Van Eps, Thomas et al. 2015), it is likely the secondary structural dynamics involving the Helical-to-Ras-like domain intersection are significantly altered, and the time-resolved anisotropy data indicate that GEF-binding results in a significant reduction in the local dynamics.

Gai1 HEXA 1 Q106C has segmental correlation times of 1.7 (-0.3, 0.3), 2.2 (-0.4, 0.4) and 1.7 (-0.3, 0.03) ns and fractions $\beta_{\text{segmental}}$ of 0.53 (-0.04, 0.03), 0.57 (-0.03, 0.03) and 0.52 (-0.03, 0.03) for the GDP, Ric-8A and GTP γ S, respectively. The nucleotide-bound states have identical correlation times and the Ric-8A state is about 30% slower, suggesting possible involvement of additional elements of structure when the GEF Ric-8A is bound. Interestingly, the cone angles calculated from the fractions $\beta_{\text{segmental}}$ are large ($\sim 40^\circ$) and independent of binding partner. Thus, the potential barrier to motion is the same with all binding partners.

Gai1 HEXA 1 K180C has segmental correlation times of 1.3 (-0.5, 0.9), 2.7 (-0.7, 0.9) and 1.8 (-0.4, 0.5) ns and fractions $\beta_{\text{segmental}}$ of 0.12 (-0.03, 0.04), 0.23 (-0.02, 0.02) and 0.30 (-0.03, 0.03) for the GDP, Ric-8A and GTP γ S, respectively. The segmental correlation time in the GDP-bound state is $\sim 40\%$ faster than in

the GTP-bound state and two-fold faster than in the Ric-8A-bound state. The fraction $\beta_{\text{segmental}}$ increases from the GDP to Ric-8A to GTP states, an indication of increased secondary structure sample-space from state to state. The observation that the GDP-bound state has the shortest segmental correlation time and the smallest fraction $\beta_{\text{segmental}}$ is consistent with a highly dynamic loop within a constrained region (i.e., smallest cone angle). The Ric-8A state with a longer $\phi_{\text{segmental}}$ suggests increased participation in local motions by residues in the neighborhood of the loop, and the \sim two-fold larger fraction $\beta_{\text{segmental}}$ suggests a substantial decrease in constraints on the loop. The GTP-bound state has a $\phi_{\text{segmental}}$ shorter than that of the Ric-8A-bound state but longer than that of the GDP-bound state, and its fraction $\beta_{\text{segmental}}$ is larger than both Ric-8A and GDP. This suggests that motions of the GTP-bound state in the region of residue K180C are more similar to those of the GDP-bound state but with the fewer structural constraints on these motions than in either the GDP-bound or Ric-8A-bound states.

Crystal structures (Coleman, Berghuis et al. 1994; Coleman and Sprang 1998) show that residue K180, which is located in switch I, is in a loop region recognized to undergo significant structural changes in different nucleotide-bound states. The segmental correlation times for the nucleotide bound states are around 1 ns and in agreement with previous EPR results (Oldham, Van Eps et al. 2007). The relatively larger uncertainty associated with the segmental correlation times in the GDP and Ric-8A-bound states might be explained by considering the dynamic nature of the switch I region. In a region that undergoes significant structural changes, it follows that large structural-dynamic state-changes would be manifested as large uncertainties in the ensemble-average measurement, as indicated by these data. Also, the Ric-8A-bound state has a substantial increase in segmental correlation time, which might be explained by considering K180C may participate in a Ric-8A-G α binding interface. G $\beta\gamma$ directly inhibits Ric-8A binding and is known to partially overlap in the switch I region (Wall, Coleman et al. 1995; Oldham, Van Eps et al. 2007) suggesting G $\beta\gamma$ may share a common binding site with Ric-8A.

Gai1 HEXA 1 K209C has segmental correlation times of 1.6 (-0.5, 0.8), 2.8 (-0.6, 0.6) and 1.0 (-0.2, 0.2) ns and fractions $\beta_{\text{segmental}}$ of 0.16 (-0.03, 0.03), 0.33 (-0.02, 0.02) and 0.33 (-0.04, 0.05) for the GDP, Ric-8A and GTP γ S respectively. The GDP-bound state segmental correlation time is longer than in the GTP-bound state (60% longer) and shorter in the Ric-8A bound state (75% shorter). This can be due to two types of dynamic processes: 1) greater structural rigidity or 2) increase in the mass and surface area of secondary structure participating in the motion. The fraction $\beta_{\text{segmental}}$ for the GDP-bound state is more than two-fold less than that of the Ric-8A and GTP-bound states; the latter states have similar fraction $\beta_{\text{segmental}}$ values. With a small fraction $\beta_{\text{segmental}}$, the GDP-bound state is sampling significantly less space compared to the Ric-8A and GTP-bound states. The GDP and GTP bound states both have correlation times around 1 ns, typical of dynamic secondary structure and similar to previous EPR results (Van Eps, Oldham et al. 2006). The $\phi_{\text{segmental}}$ of the Ric-8A bound state is much greater, 2.5 ns, possibly due to an increase in structural rigidity. However, switch II is a known G $\beta\gamma$ binding interface and inhibits Ric-8A binding (Tall, Kruminis et al. 2003). Therefore, the increase in segmental correlation time at K209C may be due to a Ric-8A-G α binding interface similar to the result found for K180C.

The $\phi_{\text{segmental}}$ of the GDP-bound state shows the largest uncertainty. This might be expected for a dynamic loop that is undergoing a structural rearrangement that is slow compared to the time-scale of the fluorescence emission (e.g., helix-coil transition) as was suggested by Hamm and Hubble from EPR spectroscopy (Van Eps, Oldham et al. 2006). This is consistent with the observation that the secondary structure of the GDP-bound state is not well resolved in crystal structures (Coleman and Sprang 1998), whereas in the GTP-bound state, this region, which is necessary for recognition by effectors, has a well-resolved helical structure (Kleuss, Raw et al. 1994; Van Eps, Thomas et al. 2015).

Gai1 HEXA 1 E238C has segmental correlation times of 1.3 (-0.2, 0.5), 1.5 (-0.3, 0.3) and 1.2 (-0.3, 0.3) ns and fractions $\beta_{\text{segmental}}$ of 0.22 (-0.03, 0.04), 0.44 (-0.02, 0.02) and 0.25 (-0.03, 0.04) for the GDP, Ric-8A

and GTP γ S respectively. The segmental correlation times for nucleotide and GEF-bound states are essentially the same. However, the fraction $\beta_{\text{segmental}}$ in the Ric-8A bound state is two-fold that of the nucleotide-bound states. The larger fraction $\beta_{\text{segmental}}$ (larger cone angle) in the Ric-8A state is an indication of increased segmental secondary-structure sample space. E238 is located in switch III of the Ras-like domain and is known to undergo structural rearrangement from the GDP to GTP state (Coleman and Sprang 1998; Van Eps, Thomas et al. 2015).

Gai1 HEXA 1 305C has segmental correlation times of 1.0 (-0.2, 0.2), 1.5 (-0.3, 0.3) and 1.2 (-0.2, 0.2) ns and fractions $\beta_{\text{segmental}}$ of 0.43 (-0.04, 0.04), 0.53 (-0.03, 0.03) and 0.72 (-0.06, 0.06) for the GDP, Ric-8A and GTP γ S bound states respectively. The segmental correlation times for nucleotide and GEF bound states are similar, indicating similar dynamic motion. However, the fraction $\beta_{\text{segmental}}$ is much greater in the GTP-bound state compared to either the GDP (67% greater) or Ric-8A (36% greater)-bound states. This indicates that this region samples the most space when in the GTP-bound state. Interestingly, this region has been shown to dramatically increase in segmental motion when bound to GTP in previous studies (Van Eps, Oldham et al. 2006) and may be a mechanism for the G α subunit dissociation from either G $\beta\gamma$ or Ric-8A following nucleotide exchange.

Gai1 HEXA 1 K330C has segmental correlation times of 1.1 (-0.2, 0.2), 2.3 (-0.5, 0.6) and 1.2 (-0.2, 0.2) ns and fractions $\beta_{\text{segmental}}$ of 0.52 (-0.04, 0.05), 0.27 (-0.02, 0.02) and 0.53 (-0.04, 0.05) for the GDP, Ric-8A and GTP γ S respectively. The GDP and GTP states have the same $\phi_{\text{segmental}}$, which is about half that for the Ric-8A-bound state, an indication of faster dynamics. The fraction $\beta_{\text{segmental}}$ for the GDP and GTP-bound states are the same and two-fold larger than for the Ric-8A bound state, an indication of a significantly larger sampling space in the nucleotide-bound states. *Gai1 K330C* is located in the $\alpha 5$ helix of the Ras-like domain which joins the C-terminus, a known binding site of GEF's, including Ric-8A (Thomas, Tall et al. 2008). Binding of a GEF at the C-terminus is highly likely to alter secondary structural

dynamic changes surrounding $\alpha 5$ and the purine ring of the guanine nucleotide that is contacted by residue 328 as indicated by these data and previous studies show increased rigidity in this region associated with GPCR binding (Oldham, Van Eps et al. 2006).

Comparison of Gai1 Mutant Depolarization Trends by Binding State: To assess the relative dynamics of each Gai1 mutant with respect to one another, segmental correlation time ($\phi_{\text{segmental}}$) and fraction $\beta_{\text{segmental}}$ heat maps were constructed. In fitting the anisotropy decays, the global rotational motion (ϕ_{global}) was calculated from the average translational diffusion coefficient ($D_{\text{translational}}$) of the Gai1 mutants and their complexes with Ric-8A, respectively, which were determined explicitly by FCS. These global rotational correlation times were input as fixed value parameters in the anisotropy decays. The segmental correlation times and fractions $\beta_{\text{segmental}}$ recovered from this fitting procedure are relative to each other and give a direct comparison of the segmental secondary structural dynamics, on the time-scale of ps-ns, that occurs within Gai1 in its various binding states. Figure 5 and 6 show the segmental correlation time and fraction $\beta_{\text{segmental}}$ heat-maps partitioned into high, medium and low values, described in the legends of the figures.

GDP-Bound State: The segmental correlation times recovered from the GDP-bound state are mostly 1.5 ns and shorter with the exception of residue Q106C and K209C which have values > 1.5 and < 2 ns.

Gai1 mutants with their depolarization contribution fraction $\beta_{\text{segmental}} < 30\%$ are Gai1 K180C, K209C and E238C. These mutants are located in the switch regions I-III. Two mutants, E63C and 305C, exhibited depolarization contribution from $30\% < \beta_{\text{segmental}} < 50\%$, and two mutants, Q106C and K330C, have depolarization contribution from $\beta_{\text{segmental}} > 50\%$.

Ric-8A-Bound State: Upon binding of Ric-8A, the majority of residues show an increase in segmental correlation times that are > 2 ns with the exception of residue E238C and 305C; both of which have segmental correlation times that remain ≤ 1.5 ns.

Residues with a depolarization contribution from fraction $\beta_{\text{segmental}}$ that stay within the same partition when binding Ric-8A from the GDP-bound state are G α i1 Q106C and K180C; Q106C $> 50\%$ and K180C is $< 30\%$. Residues which increase in contribution to depolarization with respect to fraction $\beta_{\text{segmental}}$ are G α i1 K209C, E238C and 305C; $30\% < \text{K209C, E238C} \leq 50$ and $305C > 50\%$. Residues that decrease in fraction $\beta_{\text{segmental}}$ are G α i1 E63C and K330C; $\text{E63C} < 30\%$ and $\text{K180C} < 30\%$.

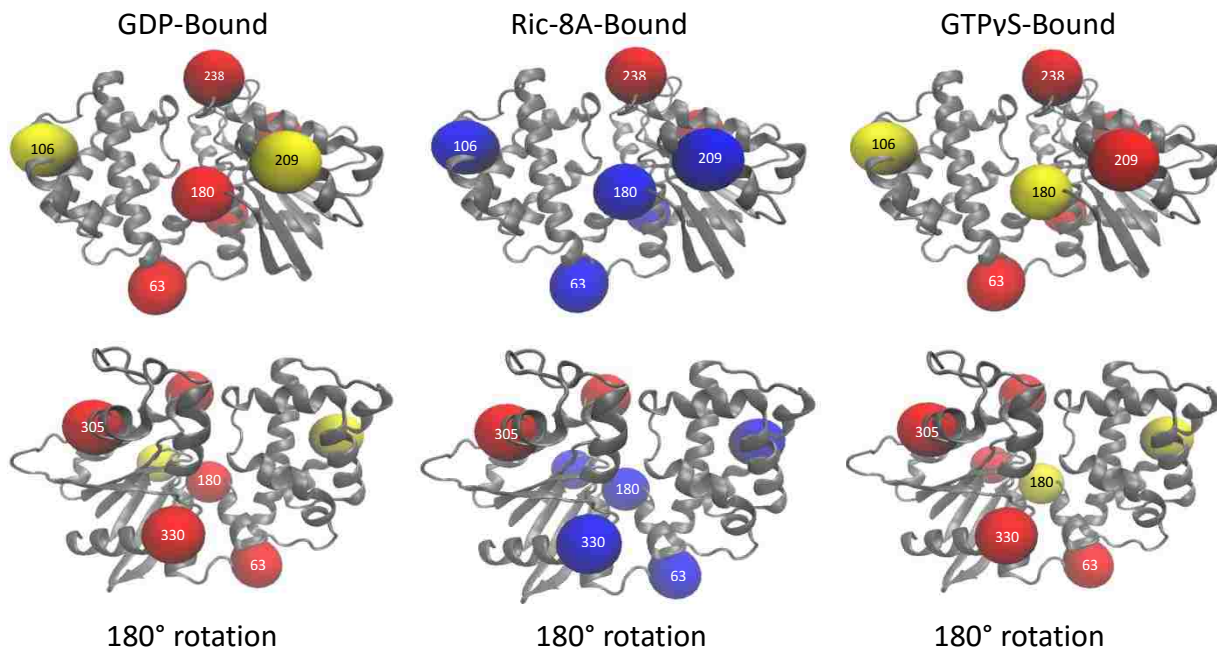


Figure 5 Heat-map constructed from segmental correlation times ($\phi_{\text{segmental}}$) extracted from the time-resolved anisotropy decay listed in table 2. Red < 1.5 ns, $1.5 \leq$ yellow < 2 ns, and blue ≥ 2 ns.

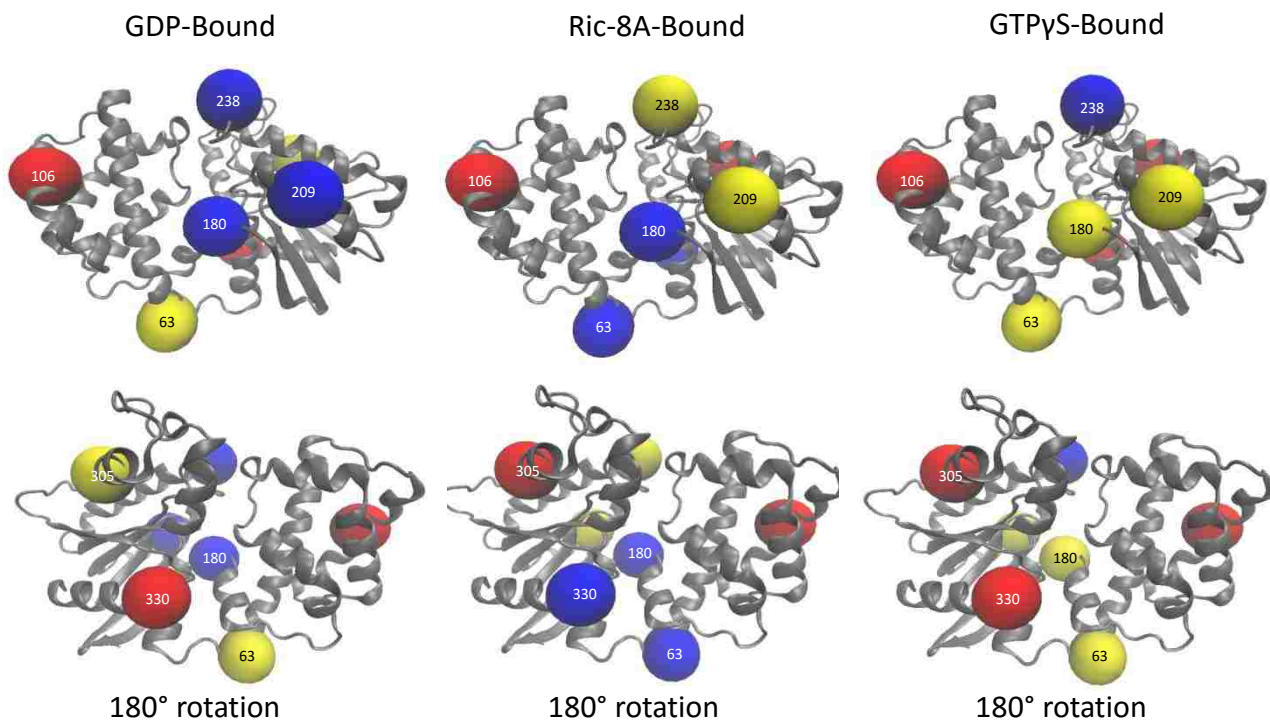


Figure 6 Heat-map constructed from segmental fraction β ($\% \beta_{\text{segmental}}$) extracted from time-resolved anisotropy decay listed in table 2. Red $> 50\%$, $30\% < \text{yellow} \leq 50$, and blue $\leq 30\%$.

To summarize, when bound to Ric-8A, an overall increase in the segmental correlation times associated with secondary structural motions and an increase in depolarization contributions attributed to larger fractions $\beta_{\text{segmental}}$ are observed in a majority of G α i1 mutants. Exceptions are E63C and K330C. Also, when bound to Ric-8A, the longer segmental correlation times, compared to the nucleotide-bound states, may indicate a Ric-8A binding interface. Furthermore, as indicated by the overall increase in contribution to depolarization associated with the fraction $\beta_{\text{segmental}}$, binding Ric-8A may cause a destabilization of the secondary structure of G α i1. Destabilization of secondary structural elements could result in formation of a molten-globular-like state. Increased mobility of larger regions of secondary structure would allow a larger sample-space in which depolarization can occur. This would appear, and is observed, as an *increase* in both the segmental correlation times and fraction $\beta_{\text{segmental}}$. In addition, comparison of the G α i1 mutants suggests that Ric-8A binding causes more destabilization in the Ras-like domain than in the Helical domain.

GTP γ S Bound State: The segmental correlation times recovered from the GTP-bound state have mostly correlation times < 1.5 ns with the exception of G α i1 Q106C and K180C. Interestingly, in the nucleotide-bound states, most mutants show a decrease in their segmental correlation times compared to the Ric-8A bound state. Exceptions are E238C and 305C, which have segmental correlation times less than 1.5 ns in all binding states. The only GTP-bound G α i1 mutants that have segmental correlation times longer than 1.5 ns are Q106C and K180C. Compared to the GDP-bound state, the segmental correlation times of the G α i1 GTP-bound state are, not surprisingly, very similar. The G α i1 mutant with their fraction $\beta_{\text{segmental}}$ in the GTP-bound state < 30% is E238C. Mutants > 30% and < 50% include E63C, K180C and K209C. Mutants > 50% are Q106C, 305C and K330C.

GTP-bound G α i1 mutants that show an increase in contribution to depolarization from $\beta_{\text{segmental}}$ with respect to the Ric-8A-bound state are E63C, K180C, and K330C. The only mutant that shows a decrease is E238C. The mutants in which depolarization from $\beta_{\text{segmental}}$ is unaffected are Q106C, K209C, and 305C.

GTP-bound G α i1 mutants that show an increase in contribution to depolarization from $\beta_{\text{segmental}}$, when compared with the GDP-bound state, are K180C, K209C, and 305C. Mutants that have the same contribution to the depolarization from $\beta_{\text{segmental}}$ are E63C, Q106C, E238C, and K330C. No mutants show a decrease in the contribution of depolarization from $\beta_{\text{segmental}}$ when compared to the GDP-bound state.

To summarize, while G α i1 mutants differ in their segmental correlation times, the correlation times of each mutant are similar when GDP is replaced with GTP. The corresponding fraction $\beta_{\text{segmental}}$ contributions are also similar with the exception that the contributions are greater for residues K180C, K209C and 305C when in the GTP-bound state.

Conclusion

The change in segmental correlation times and fraction $\beta_{\text{segmental}}$ for each mutant in their respective binding states suggests that Ric-8A binding induces a molten-globular-like state. When interacting with Ric-8A, the Ras-like domain becomes more flexible with an increased contribution of secondary structure in segmental dynamics (i.e., loop-to-helix transition, or entire helix movement, or helical bundle movement). The Helical domain, however, remains relatively unaffected. The molten-globule like character of G α i1, when in complex with Ric-8A, is associated with large domain-domain displacements (Van Eps, Thomas et al. 2015). These Ric-8A induced displacements likely involve breaking of both salt bridges and residue contacts that stabilize the di- and triphosphates of the nucleotide as well as loss of favorable van der Waals contacts with the aromatic purine ring.

Furthermore, the highly constrained $\alpha 5$ residue K330C in the Ric-8A-bound state is consistent with this helix being forced into the nucleotide binding pocket, which has been previously demonstrated for GPCR's acting as GEFs (Preininger, Funk et al. 2009). This would provide a mechanism for the increased rate of nucleotide release catalyzed by Ric-8A similar to that by a receptor.

Here we resolved the time-scales for local dynamics within secondary structural elements when G α i1 is bound to either nucleotide or the GEF Ric-8A. It is clear the times-scales of segmental dynamics are significantly perturbed when G α i1 is bound to the GEF Ric-8A. Particularly, the increase in segmental correlation times coupled with an increase in contribution to depolarization from the fraction $\beta_{\text{segmental}}$ indicates a substantial loosening of secondary structure, most noticeable in the Ras-like domain. DEER spectroscopy (Van Eps, Preininger et al. 2011; Van Eps, Thomas et al. 2015) and low-resolution H/D exchange MS (Thomas, Briknarova et al. 2011) show that GEF binding causes large-scale domain-domain displacements and increase solvent accessibility implying a molten globule-like state. The increase in intra-domain secondary structural dynamics coupled with the large-scale domain movements accounts for the dramatic increase in nucleotide exchange (10-1,000x) when G α i1 is bound to a GEF.

Chapter 3

Conformational Changes of G α

Introduction

Several years ago, we reported biophysical studies showing that Ric-8A maintains G α i1 in a structurally heterogeneous and possibly dynamic state, consistent with its chaperone-like function (Thomas, Briknarova et al. 2011). More recently, we used site-specific nitroxide spin-labeling in conjunction with DEER spectroscopy, to characterize the structural transitions that Ric-8A binding and nucleotide release induce in the structure of G α i1 (Van Eps, Thomas et al. 2015). G α proteins are members of the Ras superfamily of regulatory GTPases. Unique to G α is the insertion of a ~110 residue alpha-helical domain into Switch I of the Ras domain (Figure 2). The helical domain flanks the nucleotide binding site in the Ras domain and, while it forms few contacts with the nucleotide, serves to block its egress from the binding site. DEER experiments demonstrated that G α i1-GDP adopts a “domains-closed” conformation, whereas G α i1:Ric-8A exhibits a heterogeneous ensemble of structures with inter-domain separations spanning a ~40Å range. Ligand-activated 7-transmembrane G protein-coupled receptors (GPCRs) induce similar structural changes in G α upon catalyzing nucleotide release from heterotrimeric G proteins (Rasmussen, DeVree et al. 2011; Van Eps, Preininger et al. 2011). Ric-8A, moreover as shown in chapter 2, induces structural plasticity within the Ras domain itself, a feature not observable in the crystal structure of the β 2-Receptor:Gs complex. As shown by Van Eps et al, (Van Eps, Thomas et al. 2015), the breadth of Ras-domain distance changes increase by up to 10 Å, and there is increased structural heterogeneity in elements that define the nucleotide-binding site.

The increased number of conformational states observed in G α i1 when bound to Ric-8A suggests that the structure of G α i1 fluctuates in time. Further, the amplitude and frequency of such fluctuations in G α appear to be perturbed by its interaction with Ric-8A (Van Eps, Thomas et al. 2015) and by GPCRs (Van Eps, Preininger et al. 2011) in the nucleotide-free state and with GDP and GTP, which respectively stabilize the canonical “inactive” and “active” end-states of G α .

The aim of the present investigation is to resolve the time-scale of $G\alpha i1$ conformational dynamics using binning-time-dependent, single-molecule Förster resonance energy transfer (smFRET), and to discover how these dynamic equilibria are perturbed by activating and inactivating nucleotides, and by Ric-8A, which catalyzes nucleotide exchange, and therefore $G\alpha$ activation. We employ the 3-Gaussian (3G) model developed by Gopich and Szabo (Gopich and Szabo 2007; Gopich and Szabo 2010), which to our knowledge has not heretofore been used to investigate conformational dynamics and equilibria involved in enzyme function. We have monitored dynamics at large ($> 20 \text{ \AA}$) distance scales ($G\alpha i1$ inter-domain or intra-domain) by observation of fluctuations in FRET between pairs of donor (D) and acceptor (A) fluorophores installed at selected sites in a surface cysteine free $G\alpha i1$ construct (HEXA 1) (Medkova, Preininger et al. 2002).

The smFRET of freely diffusing $G\alpha i1$, bound to GDP, GTP or in the complex with Ric-8A, is used to measure the distribution of FRET efficiencies that inform on the number of structural states and the kinetics of the associated conformational equilibria for intra and inter-domain dynamics in $G\alpha i1$.

Methods

Protein Expression and Purification: An expression vector encoding an N-terminal, tobacco etch virus (TEV) cleavable, glutathione-S-Transferase (GST) protein $G\alpha i1$ that contained six amino acid substitutions at solvent-exposed cysteine residues (C3S-C66A-C214S-C305S-C325A-C351I) and a hexahistidine tag between amino acid residues M119 and T120 (HEXA 1) fused at its N-terminus was prepared as described (Medkova, Preininger et al. 2002; Thomas, Tall et al. 2008; Van Eps, Thomas et al. 2015). This vector was used for construction of double-cysteine mutants by QuikChange mutagenesis (Agilent): R90C-Q106C (Helical-Helical), 305C-K330C (Ras-Ras) and Q106C-E238C (Helical-Ras). $G\alpha i1$ Hexa I (hereafter, $G\alpha i1$) harboring cysteine pairs were expressed and purified as described (Thomas, Tall et al. 2008; Van Eps, Thomas et al. 2015). Also, an expression vector containing a truncated mammalian Ric-

8A (1-491) construct with a lac promoter for induction (IPTG) and a hexahistidine affinity tag was used for Ric-8A preparation previously described (Thomas, Tall et al. 2008; Thomas, Briknarova et al. 2011).

Protein Fluorescence Labeling: Double-cysteine-mutant G α i1 proteins (90-106, 106-238, 305-330) were reduced for 30 minutes (50 mM Tris pH 8.0, 250 mM NaCl, 100 μ M GDP, 10 mM DTT) at 4 °C and buffer exchanged using Millipore Amicon Ultra concentrator centrifuge tubes (30 kDa cutoff) to labeling buffer (50 mM MOPS pH 7.4, 250 mM NaCl, 100 μ M GDP). A 100-200 μ L 100- μ M reduced-protein sample was allowed to react with equimolar Alexa (C5) 488 maleimide and Alexa (C2) 647 maleimide (1 or 2, 100 nmol fluorescent dye stock aliquots from which methanol solvent was removed under vacuum) for 15 minutes at room temperature (23 °C). The reaction was quenched with the addition of β -mercapto-ethanol (β -ME) to a final concentration of 10 mM, passed over a G 10 desalting column (Invitrogen) to remove unreacted dye, and then passed through a 0.22- μ m filter to remove aggregated protein. Final concentration of Alexa-conjugated G α i1 proteins was in the range of 1-5 μ M. For smFRET analysis, 500 μ L of a 1- μ M labeled G α i1 sample in 50 mM Tris pH 8.0, 200 mM NaCl, 2 mM DTT and 10% glycerol containing either 100 μ M GDP, 1.5 μ M Ric-8A or 1.5 μ M Ric-8A+10 μ M GTP γ S+10 mM Mg²⁺, were passed over a Superdex 200 size-exclusion column at a flow rate of 0.5 mL/min using Agilent Technologies 1200 series HPLC while simultaneously monitoring 280 nm, 495 nm, and 650 nm to identify protein, Alexa 488 and Alexa 647, respectively. Fractions corresponding to 40 kDa (15.2 mL elution volume, GDP and GTP γ S-bound) or 95 kDa (12.5 mL elution volume, Ric-8A-bound) kDa were pooled and used for single-molecule spectroscopy within 24 hrs of processing. Typical final concentrations ranged from 0.5 to 1 μ M recovered protein sample.

Experimental Setup and Data Collection: Single-molecule measurements were carried out using an inverted-confocal Olympus Fluoview IX71 microscope fitted with a 60X 1.2-numerical aperture (NA) water-objective. A 480-nm pulsed-diode laser (20-60 μ W, PicoQuant) was used for excitation and

avalanche photodiodes (Perkin-Elmer Optoelectronic photocounting module model SPCM-AQR-14-FC) were used for emission detection. Donor (D) and acceptor (A) emission was routed into two channels using a 585-nm dichroic mirror with a 535/50-nm bandpass filter on the green channel (D) and a 700/50-nm bandpass filter on the red channel (A). In addition, a 640-nm diode laser (2-5 μW , PicoQuant) was used in a pulsed-interleaved excitation configuration (PIE) (Muller, Zaychikov et al. 2005) to verify and quantify stoichiometric fluorescence labeling (i.e., DD-, AA-, and DA-labeled molecules). Alexa (C5) 488 and (C2) 647 β -ME adducts were used to calibrate the confocal optical train. The molecular brightness (β) of the donor (140 ± 20 counts $\text{molec}^{-1} \text{s}^{-1} \mu\text{W}^{-1}$, $n = 3$) and acceptor (460 ± 30 counts $\text{molec}^{-1} \text{s}^{-1} \mu\text{W}^{-1}$, $n = 3$) dyes were used to estimate Γ (0.30 ± 0.06), the photon detection efficiency ratio of the donor to acceptor channel.

For data acquisition, HPLC purified double-labeled G α i1 samples were diluted to 50-100 pM in single-molecule buffers GDP, Ric-8A or GTP (50 mM Tris pH 8.0, 250 mM NaCl, 2 mM DTT, 0.05% C12E10 with the addition of either 100 μM GDP, 1 μM Ric-8A, or 10 μM GTP γ S+10 mM Mg²⁺ for each G α i1 binding state respectively). 1 mL of 50-100 pM labeled protein samples were placed in a cylindrical confocal microscope sample chamber fitted with No. 1 optical grade cylindrical disposable cover slips allowing inverted excitation and emission was collection 180° from excitation using the same optical excitation channel. Typical data collection time was 60 minutes at room temperature (21 °C), yielding 1,000-10,000 individual DA bursting events, with thousands more D/A only or weak emitting bursts filtered away. SymPhoTime v5.3.2.2 (PicoQuant) and OriginPro 9.0 software were used for data acquisition and analysis.

Ric-8A Binding and Nucleotide Exchange Assays: Freshly labeled G α i1 samples were diluted to 1 μM in 50 mM Tris pH 8.0, 250 mM NaCl, 2 mM DTT and 10% glycerol with an effective concentration of 100 μM GDP, 1.5 μM Ric-8A or 1.5 μM Ric-8A + 10 μM GTP γ S + 10 mM Mg²⁺ for each binding state respectively. The mixture was allowed to incubate on ice for 30 minutes. Each sample (1 mL) was

passed over a Superdex S200 (GE) size-exclusion column at a flow rate of 0.5 mL/min using an Agilent Technologies 1200 series HPLC and simultaneously monitored at 280 nm, 495 nm and 650 nm, resulting in separating and identifying free labeled G α i1 from Ric-8A-bound species.

Steady-State GTP Hydrolysis Assay: Freshly labeled G α i1 samples and Ric-8A were mixed resulting in effective concentrations of 1 μ M and 1.5 μ M or 2.5 μ M and 5 μ M respectively, incubate for 30 minutes on ice and then allowed to come to room temperature (23 °C). To initiate the assay, GTP + Mg²⁺ was added to the labeled G α i1, Ric-8A mixture to an effective concentration 10 μ M and 10 mM respectively and every 10 or 15 minutes 50 μ L of the reaction mixture was injected at a flow rate of 0.5 mL/min onto a Superdex S200 size-exclusion column fitted to an HPLC (Agilent Technologies series 1200). Peaks corresponding to labeled G α i:Ric-8A (12.5 mL) and free G α i (15.2 mL) were identified by monitoring at 280 nm, 495 nm and 650 nm. The ratio of labeled G α i:Ric-8A to G α i1 as a function of time for 495 and 650 nm was plotted (Appendix) and used to determine the rates of G α i1-Ric-8A reformation after GTP hydrolysis.

Fluorescence Assay of GTP Binding: Freshly prepared G α i1 (both labeled and unlabeled) were diluted to 5 μ M in 20 mM HEPES pH 8.0, 100 mM NaCl, 10 mM Mg²⁺, 0.05% C12E10 containing either 0 or 7.5 μ M Ric-8A. GTP γ S was added to the sample to a final concentration of 10 μ M, initiating the reaction. GTP γ S binding was monitored by an increase in emission intensity at 340 nm after excitation at 295 nm with 5-nm bandpass (excitation and emission) continuously for 20 min using a Perkin-Elmer LS 55 luminescence fluorimeter. Three individual data sets for each sample were globally fit to a single exponential function to recover the reaction rate using the program OriginPro 9.0. Uncertainties were calculated symmetrically at one standard deviation.

Fluorescence Correlation Spectroscopy: Fluorescence fluctuations in time, $(t) \equiv F(t) - \langle F(t) \rangle$, can be induced by a variety of processes and depend on various photophysical parameters (Muller, Chen et al.

2003; Lakowicz 2006) (Bacia and Schwille 2007). Following the treatment of Schwille *et al.* (Bacia, Haustein *et al.* 2014), the normalized fluorescence fluctuation autocorrelation function $G_{ii}(\tau)$ with lag time τ is defined as;

$$G_{ii}(\tau) = \left\langle \frac{\partial F_i(t) \partial F_i(t + \tau)}{F_i(t)} \right\rangle^2 \quad (1)$$

Assuming the fluctuations are due to changes in concentration (so-called number fluctuations), it can be described by a normalized three-dimensional (3D) diffusion autocorrelation function for species i :

$$G_{ii}(\tau) = \sum_{i=1}^n \rho_i \left(1 + \frac{\tau}{\tau_i}\right)^{-1} \left(1 + \frac{\tau}{\tau_i \kappa^2}\right)^{-\frac{1}{2}} \quad (2)$$

$\sum_{i=1}^n \rho_i = \frac{1}{\langle N \rangle}$ is the inverse of the average number of particles inside the effective measurement

volume, $V_{eff} = \pi^{\frac{2}{3}} \omega_0^2 z_0$ and $\tau_i = \frac{\omega_0^2}{4D_i}$ is defined as the average lateral diffusion time for a molecule of

species i , through V_{eff} . The ellipticity of V_{eff} is defined as $\kappa = \frac{z_0}{\omega_0}$ the ratio of vertical to horizontal radii.

Thus, an unknown diffusion coefficient can be derived from the characteristic decay time of the correlation function, τ_i , when V_{eff} is properly calibrated with a known standard. However, the shape of $G_{ii}(\tau)$ can be significantly distorted by singlet-to-triplet state conversions of the excited-state dye, that are on the same timescale as diffusion (Kasha 1947; Herkstroeter and McClure 1968; Corin, Blatt *et al.* 1987). Intersystem crossing is independent of calibration, and to account for this perturbation a “triplet” state character is input into $G_{ii}(\tau)$:

$$G_{ii}(\tau) = (1 - T + T e^{-\frac{\tau}{\tau_T}}) \sum_{i=1}^n \rho_i \left(1 + \frac{\tau}{\tau_i}\right)^{-1} \left(1 + \frac{\tau}{\tau_i \kappa^2}\right)^{-\frac{1}{2}} \quad (3)$$

and $\sum_{i=1}^n \rho_i = \frac{1}{\langle N \rangle (1 - T)}$.

There is a low probability that two molecules will be inside the confocal volume simultaneously. At longer binning times, however, it is possible to include a burst from a second molecule, and the two bursts would be counted as one event. However, increasing the binning time is a way to obtain kinetic information about dynamics (Gopich and Szabo 2007; Gopich and Szabo 2010), such as conformational-state change rates as done in this study. Therefore, to limit the possibility of binning two individual single-molecule bursts as one event, solutions were diluted to achieve burst rates less than 0.02 ms^{-1} (Appendix).

Single-molecule Förster Resonance Energy Transfer (smFRET): The efficiency of resonance energy transfer varies as the inverse sixth power of the distance between D and A and the 50% energy transfer distance for any specific D-A pair is defined as R_0 . For the FRET pair used in this study (Alexa 488-647), R_0 is 56 \AA [life technologies] (Hofig, Gabba et al. 2014). The distance-dependence of energy transfer makes FRET suitable for probing changes in structural-conformational states in a protein at the single-molecule level. FRET can be quantified in a variety of ways. At the single-molecule level, it can be defined as $N_A/(N_A + N_D)$ where N_A and N_D are the number of counts from the D and A emission intensities, respectively, for any bursting event.

3-Gaussian Model – Rates and Conformational Equilibria: In this study, the bin-time-dependent large-scale conformational state changes within Gai1 are used to extract conformational equilibria and the rate of conformational change between states. The binned data were analyzed according to the 3-Gaussian model, developed by Gopich and Szabo (Gopich and Szabo 2007; Gopich and Szabo 2010). Following their treatment, rates are obtained by fitting the FRET efficiency histogram to an approximate distribution, which for a two-state system is the sum of three-Gaussian distributions with the parameters analytically expressed in terms of the rates and FRET efficiencies given by

$$FRET \text{ Histogram } (E) = A \sum_{i=0}^2 c_i (2\pi\sigma_i^2)^{-\frac{1}{2}} \exp\left(-\frac{(E - \varepsilon_i)^2}{2\sigma_i^2}\right) \quad (4)$$

where A is the area of the histogram. The subscripts $i = 1, 2$ represent the high- and low-efficiency states, respectively. Another Gaussian function ($i = 0$) accounts for the appearance of FRET efficiency at values intermediate between those of the high and low peaks due to the transitions between the high- and low-efficiency states. The parameters for this distribution can be calculated as shown below. The three coefficients are given by,

$$c_i = p_i (e^{-k_i T}) \quad i = 1, 2 \quad (5)$$

$$c_0 = 1 - c_1 - c_2 \quad (6)$$

where T is the bin time, $p_1 = p_{\text{high}}$, $p_2 = p_{\text{low}}$, $k_1 = k_{\text{low}}$, and $k_2 = k_{\text{high}}$. Variances of the distributions are given by,

$$\sigma_i^2 = \varepsilon_i (1 - \varepsilon_i) \langle N^{-1} \rangle \quad i = 1, 2 \quad (7)$$

where $\varepsilon_1 = \varepsilon_{\text{high}}$, $\varepsilon_2 = \varepsilon_{\text{low}}$, and $\langle N^{-1} \rangle$ is the average of the inverse of the total number of photons in a bin $N = N_A + N_D$. $\langle N^{-1} \rangle$ is estimated using photon threshold limits experimentally. The mean FRET efficiency and the variance of the zeroth distribution are calculated as,

$$c_0 \varepsilon_0 = \sum_{i=1}^2 (p_i - c_i) \varepsilon_i \quad (8)$$

$$c_0 \sigma_0^2 = \frac{\langle \varepsilon \rangle_{eq} (1 - \langle \varepsilon \rangle_{eq}) \langle N^{-1} \rangle + 2p_1 p_2 (\varepsilon_1 - \varepsilon_2)^2 (kT + e^{-kT} - 1) (1 - \langle N^{-1} \rangle)}{(kT)^2 + \langle \varepsilon \rangle_{eq}^2 - \sum_{i=0}^2 c_i \varepsilon_i^2 - \sum_{i=1}^2 c_i \varepsilon \sigma_i^2} \quad (9)$$

where $\langle \varepsilon \rangle_{eq} = p_1 \varepsilon_1 + p_2 \varepsilon_2$. In eqs 4-9, $\varepsilon_{\text{high}}$, ε_{low} , $k = (k_{\text{high}} + k_{\text{low}})$, and p_{high} are fitting parameters.

Freely diffusing protein samples labeled with D and A probes generate fluorescence intensity bursts in both green and red channels. The intensity of each channel is dependent on the efficiency of the FRET event (i.e., high efficiency will produce high-red and low-green emission intensity and *vice*

versa for low efficiency). The duration of the burst intensity reflects the time the molecule remains inside the confocal volume. However, if there is a conformational change that causes a significant change in the distance between two FRET pairs, the emission intensity of each probe will also change, adding another component to the relative emission intensity. It is the time-dependent change in emission intensity due to a conformational change that is probed to quantify dynamic equilibria. To do this, the change in smFRET efficiency histograms as a function of binning time is considered.

Application of the Gopich-Szabo 3-Gaussian Model: Assuming a two-state system in dynamic equilibrium, the population distribution between the two states is determined by the relative rates at which the transitions between the two states take place. If smFRET in a freely-diffusing experiment is used to probe this two-state system, the D and A emission can be tracked as a function of time to construct a relative efficiency for any given arbitrary time period. As time increases, the probability that a dynamic two-state system will undergo a conformational change increases. When a conformational change takes place, it will be observed directly as a change in D and A emission intensities. For our analyses, if the emission count-rate exceeded 10x the average rate for a data set, it was considered a burst. Bursts were partitioned into events. Events are durations of time, or bin times, that can be set arbitrarily. In these analyses, the bin times ranged from 1,000 to 2,500 μs , which brackets the time a diffusing molecule might reside within the confocal volume. If the binning time is for a period less than the conformational transition time, then two individual states can be resolved. However, if the binning period is long (i. e., greater than the conformational transition time), then both equilibrium states will be partitioned into a single-state event, or appear as an average or “virtual” state composed of the two states in dynamic equilibrium. Figure 7 shows the theoretical time-tagged D and A emission time-trajectory (PicoQuant) for a burst partitioned into events that undergoes a conformational transition.

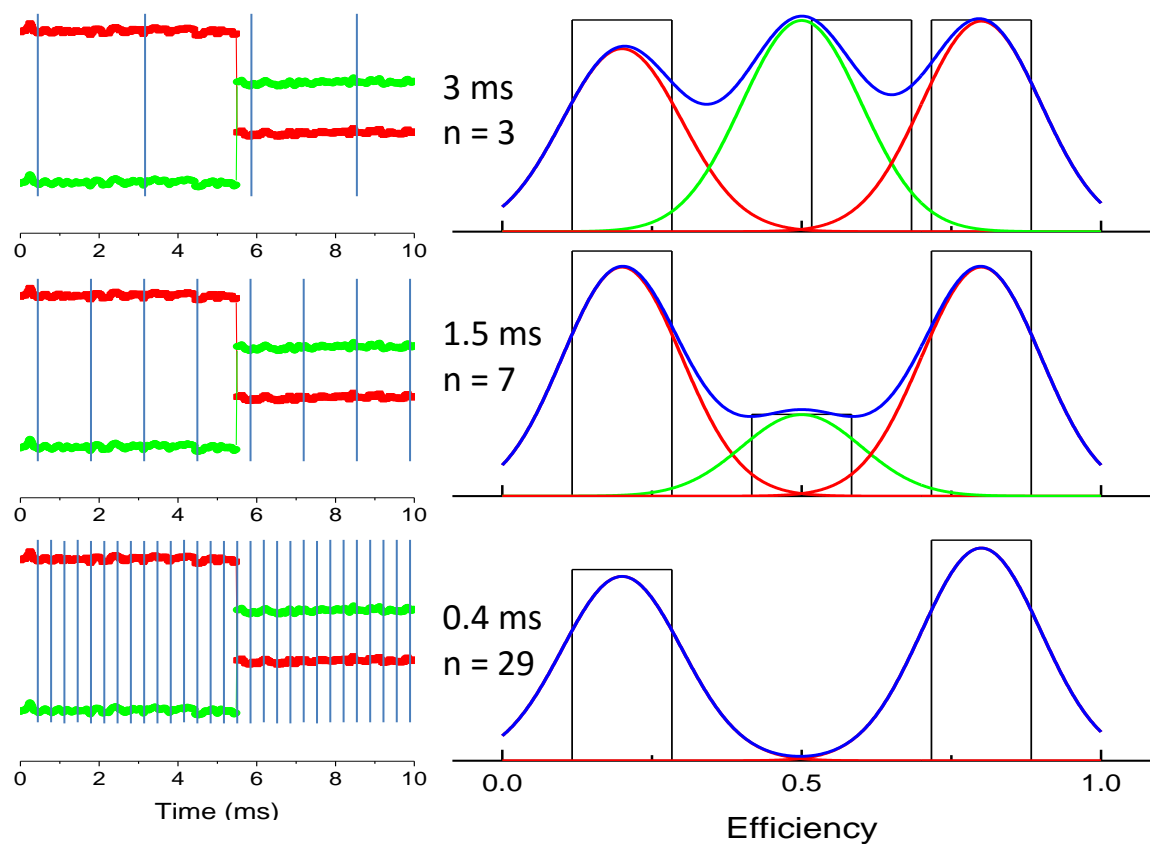


Figure 7 Theoretical burst intensity trace of both donor (green) and acceptor (red) emission for a labeled-protein undergoing a conformational change while freely diffusing through a confocal microscope setup. The intensity trace is partitioned into 3 bin times (0.4, 1.5 and 3 ms) with corresponding number of events ($n = 29, 7, 3$ respectively) and a FRET histogram is constructed for each binning time. Short binning times have many events and two- distinct states. Longer binning times have less total events and a third “virtual” state, an average of the two end states, emerges.

Construction of FRET efficiency histogram using PIE: Pulsed-interleaved-excitation (PIE) was used to discriminate molecules containing donor-only or acceptor-only labeled molecules from the molecules of interest that have both a single donor and a single acceptor (Muller, Zaychikov et al. 2005). FRET efficiency events were determined by (1) setting the photon-count-rate threshold at 10x the average of the total count rate measured during direct excitation of the acceptor, and (2) the total number of photons per event to 20, 30, 40, and 50 for 1, 1.5, 2, and 2.5 ms respectively. Briefly, in the case of a donor-only labeled molecule, when the donor-specific pulse excites the donor, the emission, quantified simultaneously in the donor and acceptor emission detection channels, would qualify this as a possible FRET event due to the total number of emission photons detected (the majority from the donor emission detector). However, direct pulsed-excitation of the donor-only labeled molecule with an acceptor-specific laser occurring within ~ 100 ns of the donor pulse would not meet the acceptor emission threshold of 10x the average acceptor count rate burst. Therefore, the labeled molecule is identified as a donor-only molecule and the associated emission burst is disqualified as a FRET event. In the case of an acceptor-only labeled molecule, a pulse from the donor laser will not produce enough total photons for the emission to qualify as a FRET event. When donor and acceptor are simultaneously present, however, there will be enough total photons from both donor and acceptor, respectively, for the event to be considered as a FRET event. Then, if the emission intensity from the acceptor met the 10x threshold, it was counted as a FRET event. Events that met these criteria were used to construct the FRET efficiency histograms. Four binning times ranging from 1,000 to 2,500 μ s were evaluated for each Gai1 mutant with its respective binding partner (GDP, GTP and Ric-8A).

Brightness-Corrected FRET-Efficiency Histograms: To obtain distance information from FRET-efficiency histograms, the relative brightness and photon detection efficiency of the optical train of the confocal setup must be balanced using a weighting factor Γ , the ratio of the molecular brightness for each channel (Roy, Hohng et al. 2008). Employing Γ corrects the FRET efficiency histogram by normalizing the

brightness of the D and A channels, giving appropriately weighted photon detection efficiency. This allows low-resolution distance information to be derived directly from the FRET-efficiency histograms. Distance histograms were generated using the software SymPho Time v.5.3.2.2.

Determination of Rates and Conformational Equilibria: The 3-Gaussian model (eq. 4-9) was employed to globally fit bin-time-dependent FRET efficiency histograms for photon binning ranging from 1,000 to 2,500 μ s. Due to the time-window limitations for observing freely-diffusing molecules using a confocal microscope setup, the transition times recovered from the 3-Gaussian model are bounded by the observation time of single-molecule emission bursts (\sim 1 to 10 ms). To obtain realistic conformational equilibria and rates (i.e., limiting the plausible conformational transition times that can be recovered to the observation time a molecule spends within the confocal volume), the slowest recoverable rate (k) of conformational transition was constrained to 0.01 ms^{-1} . In addition, the fraction of molecules in the high efficiency state (p_{high}) was constrained to $0.1 < p_{\text{high}} < 0.9$. Peak centers, p_{high} and k were globally fit as common parameters for each set of bin-time FRET efficiency histograms.

Results

Biochemical activity of Alexa-Gai1 adducts. Superdex S200 size exclusion yielded each binding state of Gai1 completely resolved when monitoring at 495 and 650 nm; addition of Ric-8A in a 1.5:1 ratio of Ric-8A:Gai1 results in the appearance of a peak at 12.5 mL elution volume and disappearance of a 15.2 mL peak (the elution volume peak of free-Gai1). Breaking of the Gai:Ric-8A complex with the addition of GTP γ S + Mg²⁺ results in the disappearance of the 12.5 mL elution volume peak and reappearance of a 15.2 mL peak. This demonstrates labeled samples both bind Ric-8A (95 ± 6 % binding, N = 6) and exchange nucleotide (91 ± 10 % dissociation, N = 6). A second size-exclusion Gai1 activity assay was developed to quantify the enzymatic hydrolysis activity using kinetic size-exclusion chromatography.

This assay shows after labeling, the GTP hydrolysis rate of Gai1 is $0.09 \pm 0.03 \text{ M min}^{-1}$ at 23°C ($N = 6$), similar to that previously reported (Tall, Krumins et al. 2003). The increase of Intrinsic tryptophan fluorescence after addition of GTP γ S demonstrated that all Gai1 samples bind GTP γ S, with and without Ric-8A present, at a rate of 0.08 ± 0.02 and $0.46 \pm 0.04 \text{ min}^{-1}$ respectively ($N = 7$ with and without Ric-8A, see Appendix for details) (Phillips and Cerione 1988; Guy, Koland et al. 1990; Medkova, Preininger et al. 2002).

Global structural changes deduced from smFRET of freely diffusing proteins: FCS was used to ensure that single-molecule conditions were met and report on the diffusion coefficients of freely diffusing labeled-proteins. The recovered diffusion coefficients of Gai1 were extracted by fitting to a triplet-character autocorrelation function (eq. 3) in the presence of saturating concentrations of nucleotide (GDP or GTP γ S) or Ric-8A were 93 ± 6 ($n = 6$) and 63 ± 10 ($n = 3$) $\mu\text{m}^2\text{s}^{-1}$, respectively (Appendix).

Without knowledge of the dipole-dipole orientation factor (κ^2), FRET does not, in general, provide high-resolution structural information (Dale and Eisinger 1976; Dale, Eisinger et al. 1979). However, taking into account the flexible linkers for the donor and acceptor probes, the Γ -weighted histograms – used here – allow low-resolution estimates of distances, which provide a basis for comparison with distances from other, higher-resolution structural methods (Hofig, Gabba et al. 2014).

The intra-Helical domain residue pair Gai1 90-106 contains one D or A dye conjugate at the end of αA (R90C) and another D or A dye conjugate in the middle of αB (Q106C). The FRET-efficiency histogram of this Gai1 conjugate has a high efficiency peak centered at 0.92, corresponding to a distance of $\sim 36 \text{ \AA}$ for GDP, Ric-8A and GTP-bound states, consistent with distances observed in crystal structures (*vide supra*). Thus, neither Ric-8A binding nor the presence of GDP vs. GTP γ S affects the structure of the Gai1 helical domain, consistent with previous DEER studies (Van Eps, Thomas et al. 2015).

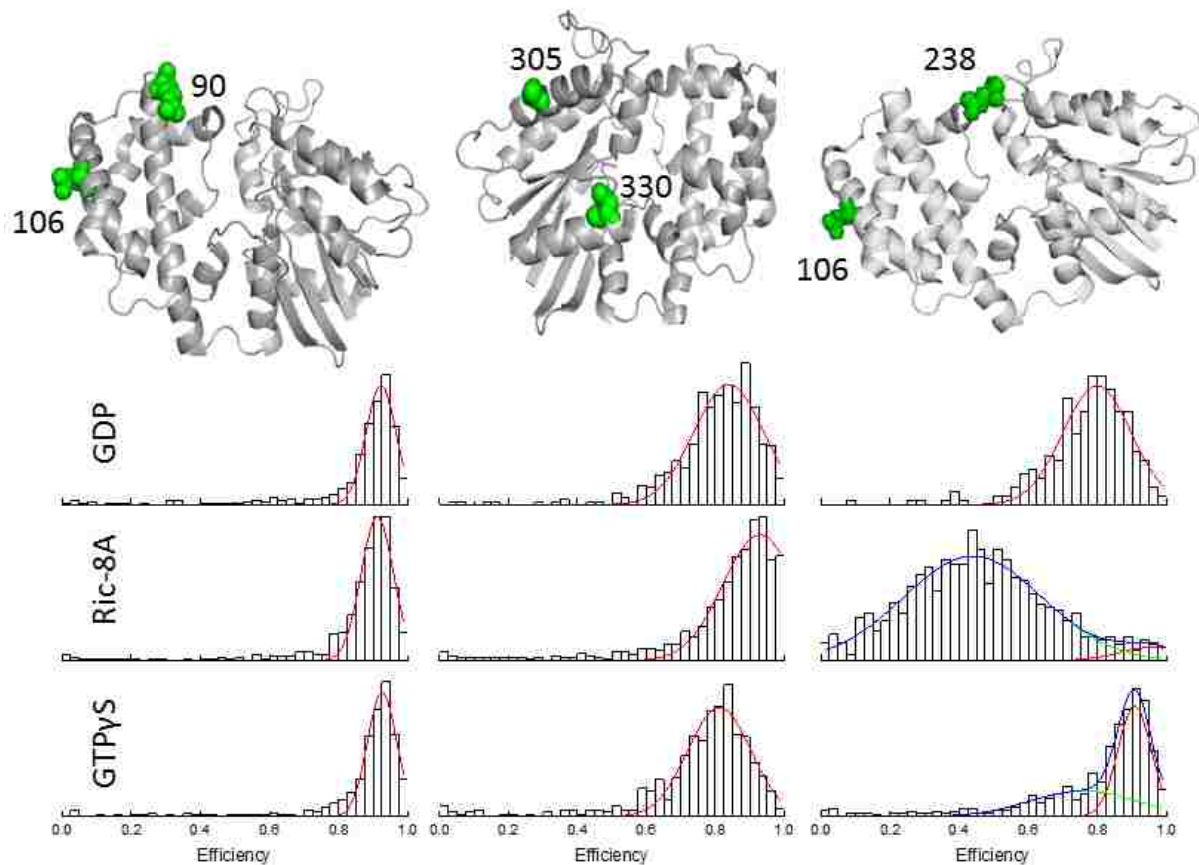


Figure 8 Donor and acceptor channel brightness-corrected (Γ -factor) FRET efficiency histograms for G α i1 90-106, G α i1 305-330, and G α i1 106-238 with binning times of 1 ms and 25 minimum photons per event. Inter-domain species displayed single (90-106) or bimodal (305-330) histogram distributions for each binding partner (GDP, Ric-8A or GTP). G α i1 90-106 all displayed a single-high efficiency peak centered at 0.92 for all binding states. G α i1 305-330 displayed efficiency peaks centered at 0.82, 0.93, and 0.80 for GDP, Ric-8A, and GTP respectively. G α i1 106-238 displayed multimodal-efficiency peaks centered at 0.83, 0.43 and 0.95, 0.76 and 0.91 for GDP, Ric-8A and GTP binding states.

G α i1 305-330 was derivatized at α 4 (305C) and at the N-terminus of α 5 (K330C), which is adjoined to the β 6- α 5 loop that engages the purine moiety of the guanine nucleotide; helix α 4 is in direct contact with α 5. The FRET-efficiency histogram of this mutant displays a single peak for all three binding states (GDP, Ric-8A and GTP γ S). However, the relative peak centers are significantly different: G α i1 305-330 peak centers at 0.84 (GDP), 0.93 (Ric-8A) and 0.81 (GTP γ S). These peaks correspond to apparent distances of 45, 39 and 43 Å, respectively. The data suggest that the Alexa 488 and Alexa 647 dyes move closer together, or reorient to generate a state of higher FRET efficiency in the nucleotide-free, Ric-8A-bound state of G α i1, than in either guanine nucleotide-bound state.

G α i1 106-238 has a mutation in α B (Q106C) of the Helical domain and a mutation in switch III (E238C) of the Ras-like domain. G α i1 106-238 displayed a single FRET-efficiency peak centered at 0.80 for the GDP-bound state, while the Ric-8A- and GTP γ S-bound states showed bimodal (possibly multimodal) FRET-efficiency histograms with peak centers at 0.95 and 0.43 for the Ric-8A-bound state and 0.91 and 0.81 for the GTP-bound state. The peak centers with population majorities for these distributions correspond to distances of 45, 59 and 37 Å for the GDP, Ric-8A and GTP-bound states respectively. Thus, the smFRET data indicate a substantial reorientation of the Helical domain with respect to the Ras domain, consistent with their spatial separation, and consistent with findings from DEER spectroscopy (Van Eps, Thomas et al. 2015). Figure (2) shows the Γ -weighted smFRET efficiency histograms for G α i1 90-106 (a), 305-330 (b) and 106-238 (c).

Dynamics of G α i1 Structural Changes: Although distance information is of interest for structural studies, our results are not dependent, *per se*, on absolute distance changes (Chung, Gopich et al. 2011). Rather, we use bin-time-dependent differences in smFRET histogram distributions to resolve conformational equilibria and determine rates for the transitions between states. The 3-Gaussian model of Gopich and Szabo (Gopich and Szabo 2007; Gopich and Szabo 2010) was used to assess G α i1 structural changes and dynamics. Conformational change rates and equilibria were obtained from global fits of bin-time-

dependent FRET efficiency histograms (binning ranging from 1,000 to 2,500 μ s). Due to the time-window limitations for observing freely-diffusing molecules using a confocal microscope setup, the transition times recovered from the 3-Gaussian model are bounded by the observation time of single-molecule emission bursts (\sim 1 to 10 ms, Appendix).

Three double-mutant Gai1 constructs are considered: 90-106 (Helical-Helical), 106-238 (Helical-Ras) and 305-330 (Ras-Ras). Table 3 gives the conformational-change rate, corresponding transition time and fraction of molecules in the high efficiency state (p_{high}) for these constructs in their respective binding states.

Intra-Domain Dynamics: The Gai1 90-106 (Helical-Helical) FRET efficiency histograms for the three binding states – GDP, GTP γ S and Ric-8A – display an asymmetric high-FRET efficiency peak centered at \sim 0.75. Fitting these data to the 3-Gaussian model, the FRET efficiency peak centers all have equilibria end-states at \sim 0.80 \pm 0.05 and 0.6 \pm 0.05 efficiency; the virtual state peak, centered at 0.75, becomes increasingly populated at longer binning times. According to the 3-Gaussian model, when the system is undergoing dynamic conformational changes during the time frame of observation, the populations from the high and low equilibrium end-states shift to the virtual state. As binning time increases the contribution of events where molecules occupy the 3rd “virtual state” also increases; this is observed as FRET efficiency peak migration from the equilibrium end state to the virtual state. The extracted transition times (T_T) for Gai1 90-106 are 5 \pm 3, 5 \pm 5 and 10 \pm 10 ms, respectively, when GDP, GTP or Ric-8A are bound (Table 3).

Gai1 305-330 (Ras-Ras-like) FRET efficiency histograms for the three binding states – GDP, GTP γ S and Ric-8A – have different FRET-efficiency distributions and show different equilibria shifts with binding partner. Bound to GDP, the peak efficiency centers are 0.77 and 0.47, with the virtual state at 0.60; the conformational transition time between the end states is 1.7 \pm 0.9 ms. When bound to Ric-8A, the 3-Gaussian fit yields equilibrium-end state peaks of 0.85 and 0.53 with a virtual peak at 0.75 and a

Gai1 90-106	GDP	Ric-8A	GTP
P_{high}	0.67 ± 0.04	0.7 ± 0.1	0.74 ± 0.03
$k \text{ (ms}^{-1}\text{)}$	0.2 ± 0.1	0.2 ± 0.2	0.1 ± 0.1
$T_{\text{T}} \text{ (ms)}$	5 ± 3	5 ± 5	10 ± 10
Gai1 305-330			
P_{high}	0.44 ± 0.02	0.52 ± 0.01	0.5 ± 0.1
$k \text{ (ms}^{-1}\text{)}$	0.6 ± 0.3	0.4 ± 0.1	1.2 ± 0.2
$T_{\text{T}} \text{ (ms)}$	1.7 ± 0.9	2.5 ± 0.6	0.8 ± 0.2
Gai1 106-238			
P_{high}	0.74 ± 0.02	0.30 ± 0.03	0.74 ± 0.01
$k \text{ (ms}^{-1}\text{)}$	1.16 ± 0.01	1.1 ± 0.2	0.33 ± 0.06
$T_{\text{T}} \text{ (ms)}$	0.80 ± 0.01	0.9 ± 0.2	3.0 ± 0.5

Table 3 Rate and equilibrium parameters recovered from the 3-Gaussian model by globally fit bin-time-dependent FRET efficiency histogram sets ranging from 1,000 to 2,500 μs using the fitting program Origin 9.0. Due to the limitations of a freely-diffusing confocal microscope setup, the transition times recovered from the 3-Gaussian model are bound by the observation time of single-molecule emission bursts, time periods of up to 10 ms. To obtain realistic conformational rates were constrained to $> 0.01 \text{ ms}^{-1}$, the upper limit of single molecules diffusing through the confocal volume. Peak centers, rates and p_{high} were globally determined using the fitting program OriginPro 9.0. Uncertainties were calculated symmetrically at one standard deviation. Three double-mutated Gai1 constructs undergoing conformational changes; Gai1 HEXA 1 90-106, 106-238, 305-330 were considered because of their relative domain-domain interactions.

conformational transition time of 2.5 ± 0.6 ms. The 3-Gaussian fit for the GTPyS-bound state yields equilibrium-end state peaks similar to the GDP-bound state at 0.79 and 0.51 FRET efficiency. The conformational transition time is 0.8 ± 0.2 ms, similar, within error, to the GDP bound state. The GTP-bound state has the lowest FRET efficiency peak while the highest FRET efficiency peak is observed in the Ric-8A-bound state. The transition times for the GDP and GTP-bound states are similar, within error, and the Ric-8A-bound state is at least 2 times slower.

Inter-Domain Dynamics: The 3-Gaussian model yields equilibrium end-state FRET-efficiency peaks at 0.66 and 0.29 with a virtual state efficiency at 0.45 and a conformational transition time of 0.80 ± 0.01 ms for the Gai1 106-238 GDP-bound state. It fits equilibrium end-state efficiency peaks at 0.55 and 0.15 with a virtual state efficiency peak at 0.30 and conformational transition time of 0.9 ± 0.2 ms for the Ric-8A-bound state. And it resolves equilibrium-end state efficiency peaks at 0.79 and 0.36 with a virtual-state efficiency peak at 0.70 and a conformational transition time of 3.0 ± 0.5 ms for the GTPyS-bound state. The GDP- and Ric-8A-bound states have similar conformational transition times and the GTP-bound state transitions are at least 3 times slower. A significantly greater distance change is observed between binding states (> 20 Å), increasing when GDP is displaced by Ric-8A and then decreasing when GTP displaces Ric-8A compared to the intra-domain mutants. Figure 9 shows bin-time dependent FRET efficiency histograms for the three double-mutant Gai1 constructs: 90-106 (Helical-Helical), 106-238 (Helical-Ras) and 305-330 (Ras-Ras) with both nucleotide and Ric-8A bound states.

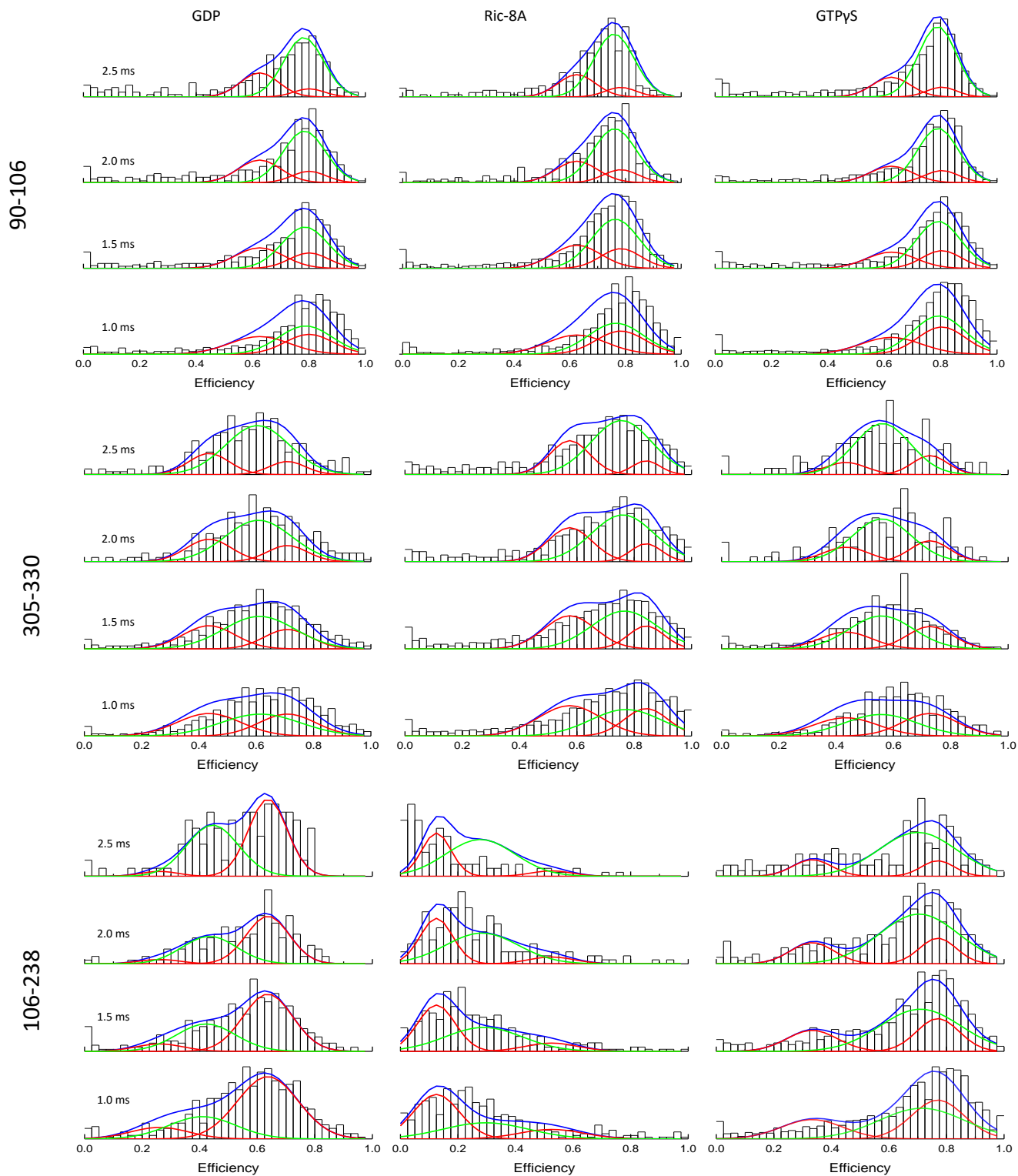


Figure 9 Time-dependent FRET efficiency histograms for intra- and inter-domain Gai1 mutants with bin-times and number of events (n) for each FRET efficiency histogram. Histograms were constructed using SymPhoTime v.5.3.2.2 software (Picoquant) where binning time (1,000 to 2,500 μ s) and 20, 30, 40, and

50 total photon per event for 1, 1.5, 2 and 2.5 ms bin times for each FRET efficiency histograms for each G α i1 mutant. The FRET efficiency histogram sets were globally fit to a 3-Gaussian model that assumes a two-conformational-state system in dynamic equilibrium represented by two Gaussian peaks at the extremities. As the bin time increases a third Gaussian peak emerges due to the bin time encompassing both the high and low efficiency states. The rate of conformational change is determined by quantifying the change in population of the low and high efficiency states on the extremities to the “virtual” 3rd state for each bin time. Table 1 shows the fitting parameters (k and p_{high}) used to generate the three Gaussians displayed in each FRET efficiency histogram.

Discussion:

The basic concepts underlying the mechanism for nucleotide exchange in G Proteins induced by GPCR GEFs are summarized in a number of reviews (Gether and Kobilka 1998; Rohrer and Kobilka 1998; Sprang and Coleman 1998; Hamm 2001; Natochin, Moussaif et al. 2001; Preininger and Hamm 2004; Kobilka 2007; Oldham and Hamm 2007; Sprang 2009; Granier and Kobilka 2012; Sprang and Elk 2012; Manglik and Kobilka 2014). Briefly, GEFs bind at the C-terminus of the alpha subunit of the G Protein heterotrimer that is partially internalized into its respective receptor. Receptor-binding of the $G\alpha$ C-terminus causes a structural rearrangement where the $\alpha 5$ helix of the Ras-like domain is compressed within the purine-nucleotide binding pocket. This causes several residue contact points within the guanine-nucleotide binding pocket to destabilize, thus decreasing nucleotide binding affinity. The destabilization of the nucleotide-binding pocket allows Helical-to-Ras-like domain interactions to also become destabilized, and large domain-domain displacements accrue, further enhancing nucleotide-exchange efficiency by exposing the binding pocket to solvent.

The structural dynamics underlying nucleotide exchange in Gai1 are not well understood although a number of studies have shown correlated secondary structural dynamics and conformational changes in the various $G\alpha$ binding states (nucleotide, $G\beta\gamma$ and the heterotrimer in complex with a receptor) (Medkova, Preininger et al. 2002; Preininger, Van Eps et al. 2003; Nanoff, Koppensteiner et al. 2006; Oldham, Van Eps et al. 2006; Ridge, Abdulaev et al. 2006; Van Eps, Oldham et al. 2006; Oldham, Van Eps et al. 2007; Kapoor, Menon et al. 2009; Preininger, Funk et al. 2009; Van Eps, Preininger et al. 2011). Here we present a first step in understanding G protein-Ric-8A dynamics by resolving the timescales for conformational transitions that could occur within and between the protein's two domains while bound to nucleotide and during nucleotide exchange mediated by the GEF Ric-8A.

Intra-domain Conformational Dynamics: G α i1 harboring Alexa-dyes at residues 90 and 106, respectively, in the α A and α B helices, monitor global structural changes within the Helical domain. In X-ray crystal structures (Kleuss, Raw et al. 1994; Wall, Coleman et al. 1995; Coleman and Sprang 1998), the backbone distance (C α to C α) between residues 90 and 106 is ~ 20 Å, consistent with the FRET distances observed in this study. DEER measurements, which are taken at 77 K, well below temperatures that allow unrestricted conformational dynamics, indicate that G α i1 and its constituent domains can reside in multiple conformations (Van Eps, Thomas et al. 2015), which suggests that to access these conformations, structural dynamics must exist at higher temperatures. The application of the 3-Gaussian model to smFRET efficiency histograms of G α i1 90-106 show that at ambient temperature the Helical domain undergoes conformational transitions on the ms time-scale.

Gopich and Szabo (Gopich and Szabo 2007; Gopich and Szabo 2010; Chung, Gopich et al. 2011) note that as binning-time increases, the probability of capturing a transition between the two high and low efficiency states increases. Thus, when a conformational state change occurs during a long binning-time, the computed FRET efficiency will reflect an average of the two states, low and high, and manifest itself as a virtual state, changing the topology of the FRET efficiency histogram. The rate of population change and conformational equilibria of the two end states generate a virtual state for G α i1 90-106 in all binding states (GDP, GTP γ S and Ric-8A); the transitions are ms and the majority populate the high efficiency state with a $p_{\text{high}} = 0.70 \pm 0.05$ for all three binding states. This indicates that the dynamics between α A and α B helices of the Helical domain are not affected by GEF activity or nucleotide binding partner.

Alexa-dyes conjugated at G α i1 residues 305 and 330, respectively in α 4 and the N-terminus of the α 5 helices report on dynamics within the Ras-like domain. The backbone distance between these two residues derived from crystal structures is ~ 26 Å, consistent with the FRET efficiency distances observed in this work. G α i1 305-330 with GDP bound displays a broad FRET efficiency distribution with

peak centers fit at 0.75 and 0.45 using the 3-Gaussian model. As the binning time increases, the equilibrium-end state peaks migrate to the virtual state, centered at 0.60. This is direct evidence that the secondary structural elements in G α i 305-330 are undergoing conformational dynamics while bound to GDP, and the population fraction in the high state, p_{high} , is 0.44, close to an equal distribution between the low and high equilibrium states. The G α i1-GTP γ S complex has a fraction population occupying the high equilibrium state of 0.50 and has two-fold faster conformational change dynamics.

The FRET efficiency histogram for G α i1 305-330 with Ric-8A bound has peaks that are at much higher efficiency than observed for the GDP- and GTP-bound states. As binning time increases, the equilibrium end states shifts in population to the virtual states similar to the nucleotide bound G α i1 305-330 states although the rate of population changes is the slowest of the three binding states.

The nature of the structural changes that accompany formation of the high-efficiency state can reflect either or both changes in the orientation of the transition dipole moments of the donor and acceptor dyes as well as in the distance between them. Consequently, the FRET data cannot be used to define the specific nature of the Ric-8A-induced structural change. Results from DEER spectroscopy indicate that spin label probes at 305 and 330 move away from each other up to 10 Å when Ric-8A displaces GDP, which supports the proposed mechanism of GEF-enhanced nucleotide exchange because 330 would move away from 305 if the α 5 helix is displaced by a translation into the nucleotide binding pocket (Preininger, Funk et al. 2009). This would not accord with the fluorescence data if changes in FRET efficiency were attributed entirely to changes in probe distance. FRET efficiency is dependent on both distance and probe orientation. Thus, a conformational change can occur that moves the D and A probes away from each other but in a more favorable orientation. This could produce an apparent high-FRET efficiency state despite a larger distance change. In any case, Ric-8A is able to induce conformational changes within the Ras-like domain that may facilitate nucleotide exchange. Notably, Ric-8A induced conformational changes occur on the millisecond timescale and are slower (3x) than in

the GTP-bound state and 40% slower than the GDP-bound state. Ric-8A may promote nucleotide release by decelerating the rate of conformational fluctuations in the Ras domain of G α i1 thereby stabilizing a conformation favorable for nucleotide release and exchange.

Inter-Domain Conformational Dynamics: Alexa-dyes conjugated at G α i1 residues 106 and 238, respectively in α B of the Helical domain and in switch III of the Ras-like domain report on dynamics of domain separation. Compared to the 90-106 and 305-330 Alexa conjugates, G α i1 106-238 undergoes large-scale, partner-dependent conformational changes. According to the smFRET, the inter-probe distance increases ~ 15 Å going from the GDP-bound to the Ric-8A-bound state and then decreases ~ 20 Å going from the Ric-8A-bound to the GTP-bound state; and the probe separation is shortest in the GTP-bound state.

G α i1 106-238 GDP-bound has equilibrium-end state peak centers at 0.65 and 0.25 and the population fraction in the high state, p_{high} , is 0.74. G α i1 106-238 GTP-bound state has equilibrium-end states at 0.75 and 0.35, similar to GDP-bound. However the rate of conformational change is much slower; at least 3 time slower. The fraction population occupying the high efficiency equilibrium-end state is the same as the GDP-bound state, 0.74. In both nucleotide-bound states, the FRET efficiency histograms show the nucleotide-bound states favor a closed domain-domain conformation.

The G α i1 106-238 Ric-8A-bound FRET efficiency histogram displays a two-conformational state system but the major population occupies the low-FRET efficiency state centered at 0.15 and the minor population state at high efficiency is centered at 0.55. This is indicative of a significant conformational change where the Ras-like and Helical domains move apart, causing a large distance separation in the FRET pairs (15 - 20 Å). This is consistent with previous structural work on G α interacting with a receptor and supports the hypothesis that nucleotide exchange is enhanced through inter-domain separation (Rasmussen, DeVree et al. 2011; Van Eps, Preiner et al. 2011).

Although there is a significant conformational change that causes domain separation associated with Ric-8A binding, the rate of conformational change is on the ms time-scale similar to conformational changes associated with secondary structural changes throughout G α . Intra-Ras domain motions are relatively slow for the GDP- and Ric-8A-bound state and increase when GTP binds and displaces Ric-8A. Interestingly, the opposite is observed for the inter-domain conformational dynamics of 106-238. Inter domain dynamics have faster conformational changes in the GDP- and Ric-8A-bound states and are much slower (3x) in the GTP bound state. This might be explained by assuming a preorganization mechanism in which Ric-8A is able to bind G α i1 and stabilize low probability or high energy states within the Ras-like domain that can efficiently exchange nucleotide, thus the conformational perturbation and slow transition time. Conversely, Ric-8A binding induces large-scale domain displacements that have relatively fast conformational dynamics between the Helical and Ras-like domains which again support a preorganization mechanism.

Conclusion

Conformational equilibria and rate changes of inter and intra-domain dynamics of G α i1 in nucleotide and Ric-8A bound states have been determined by smFRET efficiency histogram bin-time analysis developed by Gopich and Szabo (Gopich and Szabo 2007; Gopich and Szabo 2010). Multiple conformational states of G α i1 have been resolved using the 3-Gaussian model. The Helical-Helical domain conformational changes are relatively small (<5 Å), without observable influence from the binding partner (nucleotide or GEF). The intra Ras-like domain conformational changes are somewhat larger (>5 Å), and have distinct states with the GDP- and Ric-8A-bound states having slower dynamics and the GTP-bound state up to three-fold faster. Also the Ric-8A-bound state has a significant conformational change displayed as a higher FRET efficiency state, greater than GDP- or GTP-bound states. By comparison, the inter-domain (G α i1 106-238) conformational changes are much larger

(>20 Å), and exhibit distinct, multiple states that are binding-partner dependent. The time-scale of the conformational changes is ms for both intra-and inter-domain dynamics.

In conclusion, we have shown the conformational dynamics that correlate with nucleotide- and Ric-8A-bound states for inter and intra-domains which occur on the ms time-scale: (1) intra-domain motions are similar in all three binding states for the Helical domain and while bound to GDP and Ric-8A are significantly slower (up to 3x slower) in the Ras-like domain compared to GTP-bound. This is possibly due to Ric-8A stabilizing a transient conformational state that has the ability to rapidly exchange nucleotide. (2) Inter-domain conformational change timescales are similar between the GDP and Ric-8A-bound states but are up to three-fold slower when bound to GTP.

Chapter 4

Conclusion

The time-scales for secondary structural dynamics and conformational changes have been resolved around ns and ms time scales for both nucleotide (GDP and GTP) and GEF (Ric-8A)-bound states using time-resolved fluorescence anisotropy and smFRET.

The change in segmental correlation times and fraction $\beta_{\text{segmental}}$ for each mutant in their respective binding states, suggests that Ric-8A binding induces a molten-globular-like state, where the Ras-like domain becomes more flexible which allows low probability secondary structural conformations that promote nucleotide exchange which may be otherwise unlikely to occur without the aid of a GEF. Furthermore, it has been shown the molten-globule like character of G α i1 when in complex with Ric-8A, is associated with large domain-domain displacements (Van Eps, Thomas et al. 2015) that correlate with segmental dynamics resolved in this study as evidence by the highly constrained E63C residue located at the hinge region connecting the Ras-like and helical domain. Particular attention should be directed at the highly constrained α 5-N-terminus residue K330C in the Ric-8A-bound state. Constraint of this residue is consistent with the α 5 helix being displaced into the nucleotide binding pocket induced by GEF binding (Preininger, Funk et al. 2009) and suggests that Ric-8A acts in a similar manner to activated GPCRs. Finally, because G $\beta\gamma$ inhibits Ric-8A binding, it is likely the increase in the segmental correlation time of residues K180C and K209C suggests a binding interface between Ric-8A and G α contains these residues.

Conformational equilibria and rate changes of inter and intra-domain dynamics of G α i1 in nucleotide and Ric-8A-bound states determined by smFRET efficiency histogram bin-time analysis developed by Gopich and Szabo (Gopich and Szabo 2007; Gopich and Szabo 2010) shows that conformational changes occur on the ms time-scale. Multiple conformational states of G α i1 exist in both nucleotide and GEF-bound states at ambient temperature in solution. The Helical-Helical domain conformational changes are relatively small (<5 Å), without observable influence from the binding partner (nucleotide or GEF). The Ras-like domain conformational changes are somewhat larger (>5 Å),

and have distinct states with the GDP- and Ric-8A-bound states having slower conformational dynamics than the GTP-bound state. Also, a significant intra-Ras domain conformational change involving a higher FRET efficiency state is observed for Gαi1 while bound to Ric-8A. By comparison, the inter-domain conformational changes are much larger ($>20 \text{ \AA}$), and exhibit distinct, multiple states that are binding-partner dependent. This is due to Ric-8A stabilizing a transient open-conformational state that has the ability to rapidly exchange nucleotide. Inter-domain conformational change timescales are similar between the GDP and Ric-8A-bound states but are up to 3-fold slower when bound to GTP.

Together these data show Ric-8A is able to induce conformational changes that facilitate nucleotide exchange by 1) inducing large domain-domain separation between the Ras and Helical domain and 2) slowing down the conformational transition times within the Ras-like domain so that conformational states able to rapidly exchange nucleotide may be sufficiently populated.

Although these data provide insight into the mechanism of increased nucleotide exchange in Gα, there are still many aspects that remain unresolved. Particular attention should be given to the overlap, or similarities that the GEFs Ric-8A and GPCRs have. Both include large domain-domain openings where solvent is able to access the nucleotide binding pocket and both bind at the C-terminus causing an allosteric conformational change through the α5 helix in the Ras domain.

However, there are also prominent differences between the two kinds of GEFs. Ric-8A seems to be able to cause more plasticity within the Ras-like domain than GPCRs. This is a feature that might explain the slower nucleotide exchange rate of Ric-8A compared to GPCRs. Because the structure of Gα is not well-ordered when bound to Ric-8A, it may be that the enzyme is not as efficient at recognizing GTP compared to Gα-GPCR complexes. This raises the question: What future studies need to be completed to understand the differences between the GEFs Ric-8A and activated receptor? It is hypothesized that receptor and Ric-8A GEFs use similar structural perturbations to facilitate in increased

nucleotide exchange activity but the dynamics, conformational changes within the Ras-like and between the helical and Ras-like domains, are significantly different.

To resolve the structural-dynamic differences between the increased nucleotide rate of $G\alpha$ induced by Ric-8A and GPCRs, two future aims are proposed. Aim 1) Repeat the smFRET-based conformational-transition-time work for both Ric-8A and GPCRs using an immobilized or diffusion limited method in a total-internal reflectance fluorescence optical system using FRET pairs (i.e., Alexa 488 and 633, $R_0 = 45\text{\AA}$ (Invitrogen)) with an R_0 that is more sensitive to conformational changes associated with $G\alpha$ 90-106 and 305-330. The high FRET efficiency of $G\alpha$ 90-106 and 305-330 has limited efficiency resolution due to the close proximity of the probe sites. In the case of $G\alpha$ 106-238 the resolution of the efficiency histograms with Alexa 488 and 647 are reasonably resolved; however, the conformational change rates are still somewhat masked by the short observation time of freely diffusing molecules. Immobilizing or limiting the diffusion of a sample has the ability to resolve longer time-scale conformational change rates, up to seconds. It may be that the large-scale domain-domain conformational change motions are being masked by segmental motions and small-scale conformational changes that are on a much shorter timescale than absolute limiting domain-domain motions (the farthest distance change in which a domain-domain displacement takes place). Aim 2) Although we have resolved the ns and ms time scales for $G\alpha$, the dynamic motions of Ric-8A, and to a lesser degree GPCRs, are still unresolved on time-scales greater than μs . To probe the dynamics of these GEFs, it is proposed to incorporate unnatural amino acids into these proteins allowing the use the selective chemistries, e.g., click-chemistry (Ye, Kohrer et al. 2008; Naganathan, Ray-Saha et al. 2015). This affords the ability to resolve the dynamics of the GEFs without compromising their function by only having to mutate up to two residues for site-specific modifications as opposed to having to knock-out all chemically active surface cysteines within the enzyme and then introducing cysteine residues at desirable sites. Understanding the dynamics of both G proteins and GEFs in conjunction with nucleotide exchange

activity will identify the similarities between the mechanism of action for both Ric-8A and GPCRs as well as reveal their differences.

Reference list

- Afshar, K., F. S. Willard, et al. (2004). "RIC-8 is required for GPR-1/2-dependent Galpha function during asymmetric division of *C. elegans* embryos." Cell **119**(2): 219-230.
- Afshar, K., F. S. Willard, et al. (2005). "Cortical localization of the Galpha protein GPA-16 requires RIC-8 function during *C. elegans* asymmetric cell division." Development **132**(20): 4449-4459.
- Alexander, N. S., A. M. Preininger, et al. (2014). "Energetic analysis of the rhodopsin-G-protein complex links the alpha5 helix to GDP release." Nature structural & molecular biology **21**(1): 56-63.
- Alexiev, U., I. Rimke, et al. (2003). "Elucidation of the nature of the conformational changes of the EF-interhelical loop in bacteriorhodopsin and of the helix VIII on the cytoplasmic surface of bovine rhodopsin: a time-resolved fluorescence depolarization study." Journal of molecular biology **328**(3): 705-719.
- Bacia, K., E. Haustein, et al. (2014). "Fluorescence correlation spectroscopy: principles and applications." Cold Spring Harbor protocols **2014**(7): 709-725.
- Bacia, K. and P. Schwille (2007). "Fluorescence correlation spectroscopy." Methods in molecular biology **398**: 73-84.
- Bayley, P., S. Martin, et al. (2003). "Time-resolved fluorescence anisotropy studies show domain-specific interactions of calmodulin with IQ target sequences of myosin V." European biophysics journal : EBJ **32**(2): 122-127.
- Boullaran, C., O. Kamenyeva, et al. (2014). "Resistance to inhibitors of cholinesterase (Ric)-8A and Galphai contribute to cytokinesis abscission by controlling vacuolar protein-sorting (Vps)34 activity." PloS one **9**(1): e86680.
- Brochon, J. C., P. Wahl, et al. (1977). "Time resolved spectroscopy of the tryptophyl fluorescence of the *E. coli* LAC repressor." Biochemical and biophysical research communications **79**(4): 1261-1271.
- Cabrera-Vera, T. M., J. Vanhauwe, et al. (2003). "Insights into G protein structure, function, and regulation." Endocrine reviews **24**(6): 765-781.
- Chan, P., M. Gabay, et al. (2011). "Purification of heterotrimeric G protein alpha subunits by GST-Ric-8 association: primary characterization of purified G alpha(olf)." The Journal of biological chemistry **286**(4): 2625-2635.
- Chan, P., C. J. Thomas, et al. (2013). "Molecular chaperoning function of Ric-8 is to fold nascent heterotrimeric G protein alpha subunits." Proceedings of the National Academy of Sciences of the United States of America **110**(10): 3794-3799.
- Chishiki, K., S. Kamakura, et al. (2013). "Ubiquitination of the heterotrimeric G protein alpha subunits Galphai2 and Galphaq is prevented by the guanine nucleotide exchange factor Ric-8A." Biochemical and biophysical research communications **435**(3): 414-419.
- Chung, H. S., I. V. Gopich, et al. (2011). "Extracting rate coefficients from single-molecule photon trajectories and FRET efficiency histograms for a fast-folding protein." The journal of physical chemistry. A **115**(16): 3642-3656.
- Chung, K. Y., S. G. Rasmussen, et al. (2011). "Conformational changes in the G protein Gs induced by the beta2 adrenergic receptor." Nature **477**(7366): 611-615.
- Coleman, D. E., A. M. Berghuis, et al. (1994). "Structures of active conformations of Gi alpha 1 and the mechanism of GTP hydrolysis." Science **265**(5177): 1405-1412.
- Coleman, D. E., E. Lee, et al. (1994). "Crystallization and preliminary crystallographic studies of Gi alpha 1 and mutants of Gi alpha 1 in the GTP and GDP-bound states." Journal of molecular biology **238**(4): 630-634.
- Coleman, D. E. and S. R. Sprang (1996). "How G proteins work: a continuing story." Trends in biochemical sciences **21**(2): 41-44.

- Coleman, D. E. and S. R. Sprang (1998). "Crystal structures of the G protein Gi alpha 1 complexed with GDP and Mg²⁺: a crystallographic titration experiment." Biochemistry **37**(41): 14376-14385.
- Corin, A. F., E. Blatt, et al. (1987). "Triplet-state detection of labeled proteins using fluorescence recovery spectroscopy." Biochemistry **26**(8): 2207-2217.
- Couwenbergs, C., A. C. Spilker, et al. (2004). "Control of embryonic spindle positioning and Galpha activity by *C. elegans* RIC-8." Current biology : CB **14**(20): 1871-1876.
- Dale, R. E. and J. Eisinger (1976). "Intramolecular energy transfer and molecular conformation." Proceedings of the National Academy of Sciences of the United States of America **73**(2): 271-273.
- Dale, R. E., J. Eisinger, et al. (1979). "The orientational freedom of molecular probes. The orientation factor in intramolecular energy transfer." Biophysical journal **26**(2): 161-193.
- David, N. B., C. A. Martin, et al. (2005). "Drosophila Ric-8 regulates Galphai cortical localization to promote Galphai-dependent planar orientation of the mitotic spindle during asymmetric cell division." Nature cell biology **7**(11): 1083-1090.
- Dertinger, T., A. Loman, et al. (2008). "The optics and performance of dual-focus fluorescence correlation spectroscopy." Optics express **16**(19): 14353-14368.
- Deupi, X. and B. Kobilka (2007). "Activation of G protein-coupled receptors." Advances in protein chemistry **74**: 137-166.
- Figuroa, M., M. V. Hinrichs, et al. (2009). "Biophysical studies support a predicted superhelical structure with armadillo repeats for Ric-8." Protein science : a publication of the Protein Society **18**(6): 1139-1145.
- Fuentealba, J., G. Toro-Tapia, et al. (2013). "Ric-8A, a guanine nucleotide exchange factor for heterotrimeric G proteins, is critical for cranial neural crest cell migration." Developmental biology **378**(2): 74-82.
- Gabay, M., M. E. Pinter, et al. (2011). "Ric-8 proteins are molecular chaperones that direct nascent G protein alpha subunit membrane association." Science signaling **4**(200): ra79.
- Gether, U. and B. K. Kobilka (1998). "G protein-coupled receptors. II. Mechanism of agonist activation." The Journal of biological chemistry **273**(29): 17979-17982.
- Gopich, I. V. and A. Szabo (2007). "Single-molecule FRET with diffusion and conformational dynamics." The journal of physical chemistry. B **111**(44): 12925-12932.
- Gopich, I. V. and A. Szabo (2010). "FRET efficiency distributions of multistate single molecules." The journal of physical chemistry. B **114**(46): 15221-15226.
- Grams, R. R., E. A. Johnson, et al. (1972). "Laboratory data analysis system. II. Analytic error limits." American journal of clinical pathology **58**(2): 182-187.
- Granier, S. and B. Kobilka (2012). "A new era of GPCR structural and chemical biology." Nature chemical biology **8**(8): 670-673.
- Guy, P. M., J. G. Koland, et al. (1990). "Rhodopsin-stimulated activation-deactivation cycle of transducin: kinetics of the intrinsic fluorescence response of the alpha subunit." Biochemistry **29**(30): 6954-6964.
- Hamm, H. E. (2001). "How activated receptors couple to G proteins." Proceedings of the National Academy of Sciences of the United States of America **98**(9): 4819-4821.
- Hamm, H. E., S. M. Meier, et al. (2009). "Trp fluorescence reveals an activation-dependent cation-pi interaction in the Switch II region of Galphai proteins." Protein science : a publication of the Protein Society **18**(11): 2326-2335.
- Hampoelz, B., O. Hoeller, et al. (2005). "Drosophila Ric-8 is essential for plasma-membrane localization of heterotrimeric G proteins." Nature cell biology **7**(11): 1099-1105.
- Herkstroeter, W. G. and D. S. McClure (1968). "The lowest triplet state of stilbene." Journal of the American Chemical Society **90**(17): 4522-4527.

- Hinrichs, M. V., M. Torrejon, et al. (2012). "Ric-8: different cellular roles for a heterotrimeric G-protein GEF." Journal of cellular biochemistry **113**(9): 2797-2805.
- Hofig, H., M. Gabba, et al. (2014). "Inter-dye distance distributions studied by a combination of single-molecule FRET-filtered lifetime measurements and a weighted accessible volume (wAV) algorithm." Molecules **19**(12): 19269-19291.
- Holinstat, M., W. M. Oldham, et al. (2006). "G-protein-coupled receptors: evolving views on physiological signalling: symposium on G-protein-coupled receptors: evolving concepts and new techniques." EMBO reports **7**(9): 866-869.
- Jenie, R. I., M. Nishimura, et al. (2013). "Increased ubiquitination and the crosstalk of G protein signaling in cardiac myocytes: involvement of Ric-8B in Gs suppression by Gq signal." Genes to cells : devoted to molecular & cellular mechanisms **18**(12): 1095-1106.
- Kapoor, N., S. T. Menon, et al. (2009). "Structural evidence for a sequential release mechanism for activation of heterotrimeric G proteins." Journal of molecular biology **393**(4): 882-897.
- Kasha, M. (1947). "Phosphorescence and the role of the triplet state in the electronic excitation of complex molecules." Chemical reviews **41**(2): 401-419.
- Kaya, A. I., A. D. Lokits, et al. (2014). "A conserved phenylalanine as a relay between the alpha5 helix and the GDP binding region of heterotrimeric Gi protein alpha subunit." The Journal of biological chemistry **289**(35): 24475-24487.
- Kim, T. Y., T. Schlieter, et al. (2012). "Activation and molecular recognition of the GPCR rhodopsin-- insights from time-resolved fluorescence depolarisation and single molecule experiments." European journal of cell biology **91**(4): 300-310.
- Kinosita, K., Jr., A. Ikegami, et al. (1982). "On the wobbling-in-cone analysis of fluorescence anisotropy decay." Biophysical journal **37**(2): 461-464.
- Kleuss, C., A. S. Raw, et al. (1994). "Mechanism of GTP hydrolysis by G-protein alpha subunits." Proceedings of the National Academy of Sciences of the United States of America **91**(21): 9828-9831.
- Kobilka, B. K. (2007). "G protein coupled receptor structure and activation." Biochimica et biophysica acta **1768**(4): 794-807.
- Lakowicz, J. R. (2006). Principles of Fluorescence. New York, Springer.
- Lakowicz, J. R. (2006). Principles of Fluorescence Spectroscopy. New York, Springer.
- Ma, S., H. J. Kwon, et al. (2012). "Ric-8a, a guanine nucleotide exchange factor for heterotrimeric G proteins, regulates bergmann glia-basement membrane adhesion during cerebellar foliation." The Journal of neuroscience : the official journal of the Society for Neuroscience **32**(43): 14979-14993.
- Manglik, A. and B. Kobilka (2014). "The role of protein dynamics in GPCR function: insights from the beta2AR and rhodopsin." Current opinion in cell biology **27**: 136-143.
- Marin, E. P., A. G. Krishna, et al. (2001). "Rapid activation of transducin by mutations distant from the nucleotide-binding site: evidence for a mechanistic model of receptor-catalyzed nucleotide exchange by G proteins." The Journal of biological chemistry **276**(29): 27400-27405.
- Marin, E. P., A. G. Krishna, et al. (2002). "Disruption of the alpha5 helix of transducin impairs rhodopsin-catalyzed nucleotide exchange." Biochemistry **41**(22): 6988-6994.
- Medina, M. A. and P. Schwille (2002). "Fluorescence correlation spectroscopy for the detection and study of single molecules in biology." BioEssays : news and reviews in molecular, cellular and developmental biology **24**(8): 758-764.
- Medkova, M., A. M. Preininger, et al. (2002). "Conformational changes in the amino-terminal helix of the G protein alpha(i1) following dissociation from Gbetagamma subunit and activation." Biochemistry **41**(31): 9962-9972.

- Miller, K. G., A. Alfonso, et al. (1996). "A genetic selection for *Caenorhabditis elegans* synaptic transmission mutants." Proceedings of the National Academy of Sciences of the United States of America **93**(22): 12593-12598.
- Miller, K. G., M. D. Emerson, et al. (2000). "RIC-8 (Synembryn): a novel conserved protein that is required for G(q)alpha signaling in the *C. elegans* nervous system." Neuron **27**(2): 289-299.
- Miller, K. G. and J. B. Rand (2000). "A role for RIC-8 (Synembryn) and GOA-1 (G(o)alpha) in regulating a subset of centrosome movements during early embryogenesis in *Caenorhabditis elegans*." Genetics **156**(4): 1649-1660.
- Minazzo, A. S., R. C. Darlington, et al. (2009). "Loop dynamics of the extracellular domain of human tissue factor and activation of factor VIIa." Biophysical journal **96**(2): 681-692.
- Muller, B. K., E. Zaychikov, et al. (2005). "Pulsed interleaved excitation." Biophysical journal **89**(5): 3508-3522.
- Muller, C. B., K. Weiss, et al. (2008). "Calibrating differential interference contrast microscopy with dual-focus fluorescence correlation spectroscopy." Optics express **16**(6): 4322-4329.
- Muller, J. D., Y. Chen, et al. (2003). "Fluorescence correlation spectroscopy." Methods in enzymology **361**: 69-92.
- Nagai, Y., A. Nishimura, et al. (2010). "Ric-8B stabilizes the alpha subunit of stimulatory G protein by inhibiting its ubiquitination." The Journal of biological chemistry **285**(15): 11114-11120.
- Naganathan, S., S. Ray-Saha, et al. (2015). "Multiplex detection of functional G protein-coupled receptors harboring site-specifically modified unnatural amino acids." Biochemistry **54**(3): 776-786.
- Nanoff, C., R. Koppensteiner, et al. (2006). "The carboxyl terminus of the Galpha-subunit is the latch for triggered activation of heterotrimeric G proteins." Molecular pharmacology **69**(1): 397-405.
- Natochin, M., M. Moussaif, et al. (2001). "Probing the mechanism of rhodopsin-catalyzed transducin activation." Journal of neurochemistry **77**(1): 202-210.
- Nishimura, A., M. Okamoto, et al. (2006). "Ric-8A potentiates Gq-mediated signal transduction by acting downstream of G protein-coupled receptor in intact cells." Genes to cells : devoted to molecular & cellular mechanisms **11**(5): 487-498.
- Oldham, W. M. and H. E. Hamm (2007). "How do receptors activate G proteins?" Advances in protein chemistry **74**: 67-93.
- Oldham, W. M. and H. E. Hamm (2008). "Heterotrimeric G protein activation by G-protein-coupled receptors." Nature reviews. Molecular cell biology **9**(1): 60-71.
- Oldham, W. M., N. Van Eps, et al. (2006). "Mechanism of the receptor-catalyzed activation of heterotrimeric G proteins." Nature structural & molecular biology **13**(9): 772-777.
- Oldham, W. M., N. Van Eps, et al. (2007). "Mapping allosteric connections from the receptor to the nucleotide-binding pocket of heterotrimeric G proteins." Proceedings of the National Academy of Sciences of the United States of America **104**(19): 7927-7932.
- Phillips, W. J. and R. A. Cerione (1988). "The intrinsic fluorescence of the alpha subunit of transducin. Measurement of receptor-dependent guanine nucleotide exchange." The Journal of biological chemistry **263**(30): 15498-15505.
- Posner, B. A., M. B. Mixon, et al. (1998). "The A326S mutant of Galpha1 as an approximation of the receptor-bound state." The Journal of biological chemistry **273**(34): 21752-21758.
- Preininger, A. M., M. A. Funk, et al. (2009). "Helix dipole movement and conformational variability contribute to allosteric GDP release in Galphai subunits." Biochemistry **48**(12): 2630-2642.
- Preininger, A. M. and H. E. Hamm (2004). "G protein signaling: insights from new structures." Science's STKE : signal transduction knowledge environment **2004**(218): re3.
- Preininger, A. M., J. Parello, et al. (2008). "Receptor-mediated changes at the myristoylated amino terminus of Galpha(ii) proteins." Biochemistry **47**(39): 10281-10293.

- Preininger, A. M., N. Van Eps, et al. (2003). "The myristoylated amino terminus of Galpha(i)(1) plays a critical role in the structure and function of Galpha(i)(1) subunits in solution." Biochemistry **42**(26): 7931-7941.
- Rasmussen, S. G., B. T. DeVree, et al. (2011). "Crystal structure of the beta2 adrenergic receptor-Gs protein complex." Nature **477**(7366): 549-555.
- Raw, A. S., D. E. Coleman, et al. (1997). "Structural and biochemical characterization of the GTPgammaS-, GDP.Pi-, and GDP-bound forms of a GTPase-deficient Gly42 --> Val mutant of Galpha1." Biochemistry **36**(50): 15660-15669.
- Ridge, K. D., N. G. Abdulaev, et al. (2006). "Conformational changes associated with receptor-stimulated guanine nucleotide exchange in a heterotrimeric G-protein alpha-subunit: NMR analysis of GTPgammaS-bound states." The Journal of biological chemistry **281**(11): 7635-7648.
- Ries, J. and P. Schwille (2012). "Fluorescence correlation spectroscopy." BioEssays : news and reviews in molecular, cellular and developmental biology **34**(5): 361-368.
- Rohrer, D. K. and B. K. Kobilka (1998). "G protein-coupled receptors: functional and mechanistic insights through altered gene expression." Physiological reviews **78**(1): 35-52.
- Roy, R., S. Hohng, et al. (2008). "A practical guide to single-molecule FRET." Nature methods **5**(6): 507-516.
- Schroder, G. F., U. Alexiev, et al. (2005). "Simulation of fluorescence anisotropy experiments: probing protein dynamics." Biophysical journal **89**(6): 3757-3770.
- Seifert, R., K. Wenzel-Seifert, et al. (1999). "GPCR-Galpha fusion proteins: molecular analysis of receptor-G-protein coupling." Trends in pharmacological sciences **20**(9): 383-389.
- Shukla, A. K., A. Manglik, et al. (2013). "Structure of active beta-arrestin-1 bound to a G-protein-coupled receptor phosphopeptide." Nature **497**(7447): 137-141.
- Small, E. W. and I. Isenberg (1977). "Hydrodynamic properties of a rigid molecule: rotational and linear diffusion and fluorescence anisotropy." Biopolymers **16**(9): 1907-1928.
- Sprang, S. (2001). "GEFs: master regulators of G-protein activation." Trends in biochemical sciences **26**(4): 266-267.
- Sprang, S. R. (1995). "How Ras works: structure of a Rap-Raf complex." Structure **3**(7): 641-643.
- Sprang, S. R. (1997). "G protein mechanisms: insights from structural analysis." Annual review of biochemistry **66**: 639-678.
- Sprang, S. R. (1997). "G proteins, effectors and GAPs: structure and mechanism." Current opinion in structural biology **7**(6): 849-856.
- Sprang, S. R. (1997). "GAP into the breach." Science **277**(5324): 329-330.
- Sprang, S. R. (2007). "Structural biology: a receptor unlocked." Nature **450**(7168): 355-356.
- Sprang, S. R. (2009). Handbook of Cell Signaling. R. A. Bradshaw and E. A. Dennis. New York, Academic Press. **3**.
- Sprang, S. R. and D. E. Coleman (1998). "Invasion of the nucleotide snatchers: structural insights into the mechanism of G protein GEFs." Cell **95**(2): 155-158.
- Sprang, S. R. and J. C. Elk (2012). "Cell signaling. Structural origins of receptor bias." Science **335**(6072): 1055-1056.
- Tall, G. G. (2013). "Ric-8 regulation of heterotrimeric G proteins." Journal of receptor and signal transduction research **33**(3): 139-143.
- Tall, G. G. and A. G. Gilman (2004). "Purification and functional analysis of Ric-8A: a guanine nucleotide exchange factor for G-protein alpha subunits." Methods in enzymology **390**: 377-388.
- Tall, G. G., A. M. Krumin, et al. (2003). "Mammalian Ric-8A (synembryn) is a heterotrimeric Galpha protein guanine nucleotide exchange factor." The Journal of biological chemistry **278**(10): 8356-8362.

- Tall, G. G., B. R. Patel, et al. (2013). "Ric-8 folding of G proteins better explains Ric-8 apparent amplification of G protein-coupled receptor signaling." Proceedings of the National Academy of Sciences of the United States of America **110**(34): E3148.
- Tesmer, J. J., D. M. Berman, et al. (1997). "Structure of RGS4 bound to AIF4--activated G(i alpha1): stabilization of the transition state for GTP hydrolysis." Cell **89**(2): 251-261.
- Thomas, C. J., K. Briknarova, et al. (2011). "The nucleotide exchange factor Ric-8A is a chaperone for the conformationally dynamic nucleotide-free state of Galphai1." PloS one **6**(8): e23197.
- Thomas, C. J., G. G. Tall, et al. (2008). "Ric-8A catalyzes guanine nucleotide exchange on G alpha1 bound to the GPR/GoLoco exchange inhibitor AGS3." The Journal of biological chemistry **283**(34): 23150-23160.
- Tonisssoo, T., S. Lulla, et al. (2010). "Nucleotide exchange factor RIC-8 is indispensable in mammalian early development." Developmental dynamics : an official publication of the American Association of Anatomists **239**(12): 3404-3415.
- Tonisssoo, T., R. Meier, et al. (2003). "Expression of ric-8 (synembryn) gene in the nervous system of developing and adult mouse." Gene expression patterns : GEP **3**(5): 591-594.
- Van Eps, N., W. M. Oldham, et al. (2006). "Structural and dynamical changes in an alpha-subunit of a heterotrimeric G protein along the activation pathway." Proceedings of the National Academy of Sciences of the United States of America **103**(44): 16194-16199.
- Van Eps, N., A. M. Preininger, et al. (2011). "Interaction of a G protein with an activated receptor opens the interdomain interface in the alpha subunit." Proceedings of the National Academy of Sciences of the United States of America **108**(23): 9420-9424.
- Van Eps, N., C. J. Thomas, et al. (2015). "The guanine nucleotide exchange factor Ric-8A induces domain separation and Ras domain plasticity in Galphai1." Proceedings of the National Academy of Sciences of the United States of America **112**(5): 1404-1409.
- Vellano, C. P., E. M. Maher, et al. (2011). "G protein-coupled receptors and resistance to inhibitors of cholinesterase-8A (Ric-8A) both regulate the regulator of g protein signaling 14 RGS14.Galphai1 complex in live cells." The Journal of biological chemistry **286**(44): 38659-38669.
- Wall, M. A., D. E. Coleman, et al. (1995). "The structure of the G protein heterotrimer Gi alpha 1 beta 1 gamma 2." Cell **83**(6): 1047-1058.
- Wall, M. A., B. A. Posner, et al. (1998). "Structural basis of activity and subunit recognition in G protein heterotrimers." Structure **6**(9): 1169-1183.
- Woodard, G. E., N. N. Huang, et al. (2010). "Ric-8A and Gi alpha recruit LGN, NuMA, and dynein to the cell cortex to help orient the mitotic spindle." Molecular and cellular biology **30**(14): 3519-3530.
- Ye, S., C. Kohrer, et al. (2008). "Site-specific incorporation of keto amino acids into functional G protein-coupled receptors using unnatural amino acid mutagenesis." The Journal of biological chemistry **283**(3): 1525-1533.

Appendix

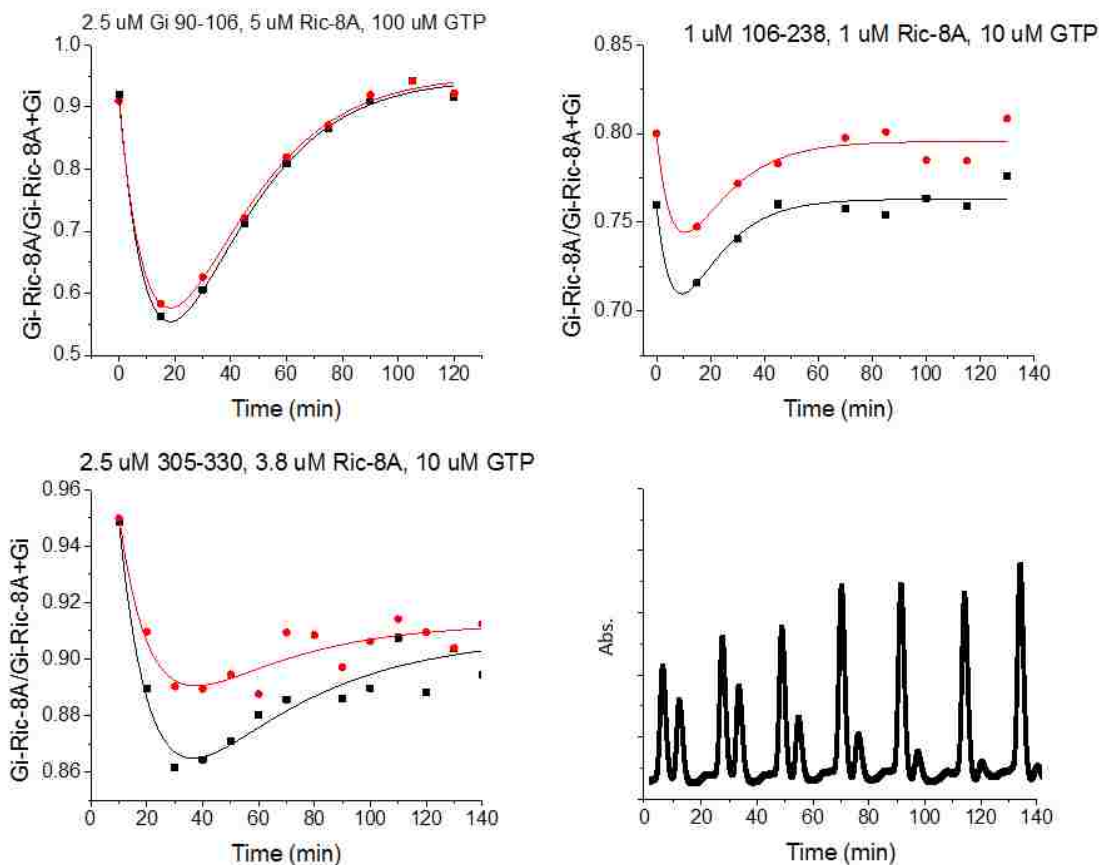


Figure 1 (supplementary): GTP hydrolysis assay, freshly labeled Gai1 samples were diluted to 1 and 2.5 uM. 1.5 or 5 uM Ric-8A was added to the solution and allowed to incubate for 30 min on ice. To initiate the assay, 10 uM GTP+10 mM Mg²⁺ was added to the Gai1+Ric-8A samples and every 10 or 15 min 50 uL of the reaction mixture was injected onto a Superdex 200 size-exclusion column. Peaks corresponding to Gai1-Ric-8A and free Gai1 were simultaneously monitored at 280 nm, 495 nm and 650 nm. The ratio Gai1-Ric-8A to Gai1 as a function of time for each wavelength was plotted and used to confirm Ric-8AGai1 formation and thus GTP hydrolysis at a rate of $0.09 \pm 0.03 \text{ M min}^{-1}$ @ 23°C. Superdex S200 size-exclusion abs @ 650 nm trace of Gai1 90-106 double labeled with Alexa 488 and 647 mixed with Ric-8A. 50 uL aliquots of the preincubated (1 hr @ 4 °C) mixture of 1 uM labeled protein, 1.5 uM Ric-8A and 10 uM GTP in buffer (50 mM Tris pH 8.0, 250 mM NaCl, 10 mM Mg²⁺, 2 mM DTT and 10% glycerol) were injected on to a Superdex S200 sizing column every 15 minutes for 150 min. The peak area ratio of Ric-8A:Gai1 to free Gai1 was used to determine the rate of Ric-8A: Gai1 reformation following GTP consumption.

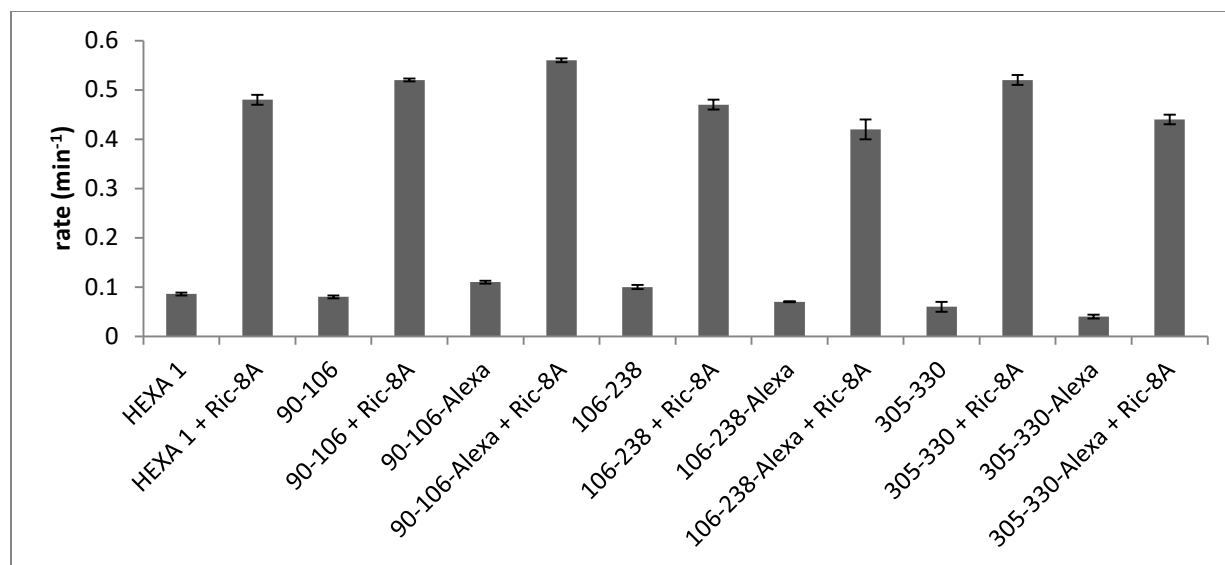


Figure 2 (supplementary): Rates of GTP γ S binding for Gai1 samples with and without Ric-8A present. The increase in intrinsic tryptophan fluorescence of a 5 μ M Gai1 sample in assay buffer (20 mM HEPES pH 8.0, 100 mM NaCl, 10 mM Mg²⁺, 2 mM DTT and 0.05% C12E10) due to GTP γ S (10 μ M) binding was monitored for a 20 min period with and without Ric-8A present in a 1:1.5 ratio respectively. The computed binding rate was determined by globally fitting 3 individual curves from each sample to a single exponential in the fitting program OriginPro 9.0.

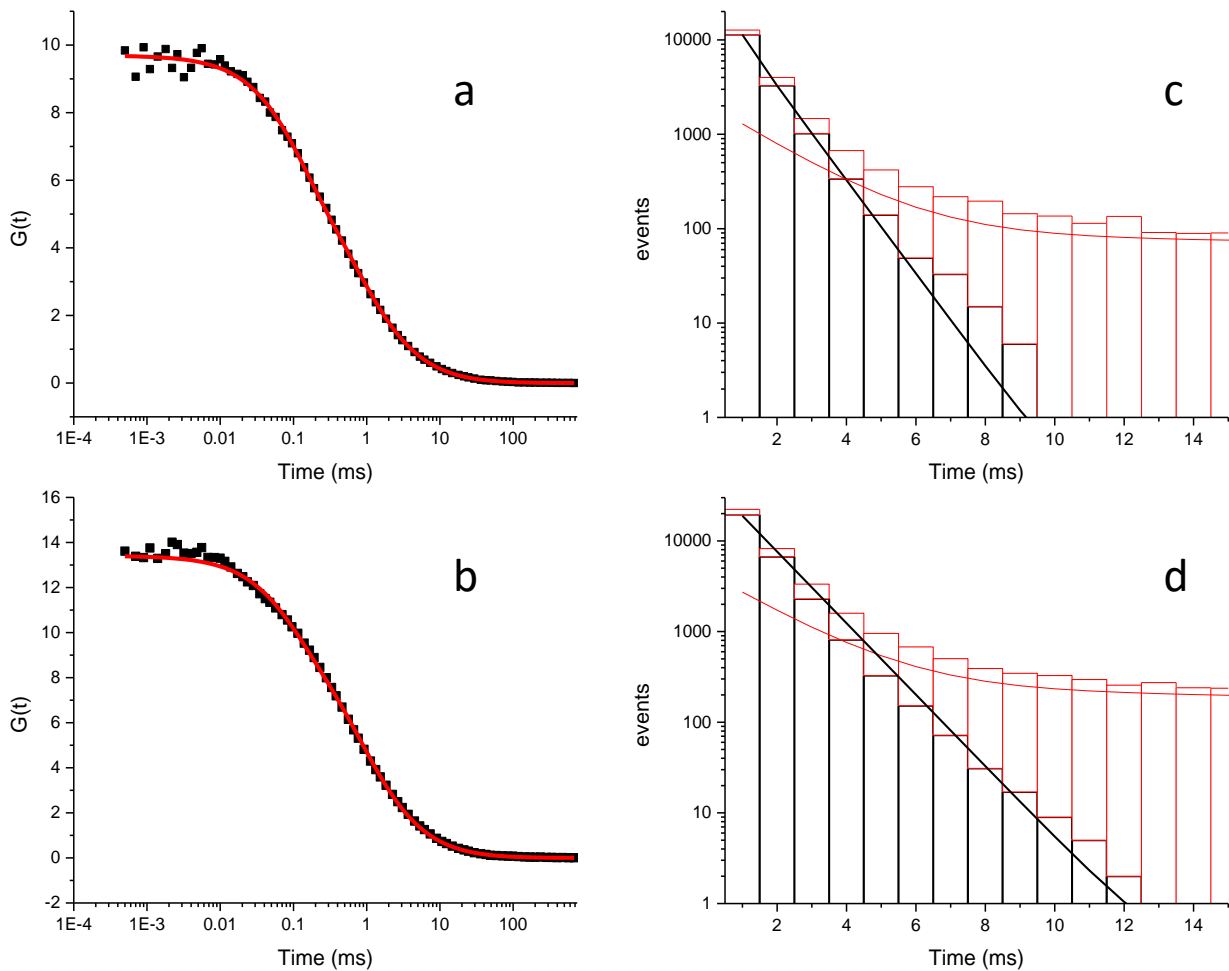


Figure 3 (supplementary): Auto-correlation of the green (D) channel for freely diffusing double-labeled Gai1 mutants in the GDP/GTP γ S(a)- or Ric-8A(b)-bound state and burst (both green and red channels) duration histograms of double-labeled Gai1 mutants in the GDP/GTP γ S(c)- or Ric-8A(d)-bound state. Auto correlation curves were fit (OriginPro 9.0) to a single-species triplet-state function yielding diffusion coefficients of $\sim 93 \pm 6$ (a) and 63 ± 10 (b) $\mu\text{m}^2 \text{s}^{-1}$ for Gai1 and Gai1:Ric-8A respectively. Burst duration histograms show the persistence time of a donor or acceptor emission from a fluorescently labeled molecule diffusing through the confocal volume. The duration of the burst is dependent on the shape and size of the molecule diffusing through the confocal volume. The dark-state (time in-between burst) persistence time histogram is shown in red for c and d. Fitting the dark-state persistence time to a single-exponential yields decay times greater than 50 ms (c and d, red) ensuring single-molecule conditions are held for binning times greater than 10 ms, the longest binning time considered in this work.

	Diffusion Coefficient ($\mu\text{m}^2 \text{s}^{-1}$)	τ_D (ms)
Gai1 90-106		
GDP	95 (-5, 5)	0.60 (-0.03, 0.03)
GTP	90 (-6, 6)	0.63 (-0.04, 0.04)
Ric-8A	74 (-6, 7)	0.77 (-0.06, 0.07)
Gai1 305-330		
GDP	98 (-8, 9)	0.38 (-0.03, 0.04)
GTP	92 (-10, 12)	0.43 (-0.04, 0.05)
Ric-8A	57 (-4, 4)	0.86 (-0.06, 0.06)
Gai1 106-238		
GDP	90 (-4, 4)	0.66 (-0.03, 0.03)
GTP	93 (-5, 6)	0.54 (-0.03, 0.03)
Ric-8A	69 (-6, 7)	0.75 (-0.07, 0.08)

Table 1. Diffusion coefficients and diffusion times for inter- and intra- domain Gai1 mutants determined by fitting a triplet-character correlation function to FCS curves. Uncertainties were calculated using the support-plane method using the program SymPho Time v. 5.3.2.2.

